### Chapter 15

# Modern Techniques, Modern Concepts, and Molecules Doing Stuff

Robert W. Field\*,1 and Arthur G. Suits2

<sup>1</sup>Department of Chemistry, Massachusetts Institute of Technology, Cambridge, Massachusetts 02139, United States

<sup>2</sup>Department of Chemistry, University of Missouri, 601 S. College Avenue, Columbia, Missouri 65211, United States

\*Email: rwfield@mit.edu.

Recent experimental advances in frequency-domain spectroscopy have resulted in large increases in the quantity, quality, relative intensities, and inter-species correlated rotation-vibration population distributions. When a spectrum is recorded without scanning a laser or a monochromator, it can yield meaningful, information-rich relative intensities. We discuss a series of examples in this paper. This series culminates in two examples of multiplexed spectra: Chirped Pulse millimeter-wave Spectroscopy and Velocity Map Imaging. A few-us duration chirped pulse of millimeter-wave radiation is generated electronically without appreciable pulse-to-pulse variation of either the pulse itself or the system to which it is applied. A velocity map image is collected event-by-event on a 2-dimensional detector, without significant variation of the laser frequencies that generate the detected species. The availability of new classes of experimental data have led to the asking and answering of previously unimaginable questions about the structure and dynamics of small molecules at high levels of internal excitation, especially in explicitly targeted regions of state-space. Spectra are assigned based on observation or reconstruction of simple **patterns**. These patterns are broken by spectroscopic perturbations. The **broken patterns** can be collected and arranged into a higher level of pattern: a pattern of broken patterns. These perturbations can be interactions of an electronic "bright state" with multiple vibrational levels of several electronic excited "dark" states or, for the 3N-6 vibrational normal modes of an N-atom polyatomic molecule, vibrational polyads. Polyads are much more robust than vibrational normal modes because, as excitation energy increases, the values of the matrix elements and the dimension of the Heff polyad matrices depend in a simple, a priori known manner on the polyad quantum numbers. At high excitation energy, the energy and structure of transition states for isomerization become encoded in a broken pattern of broken patterns, for example, the transition state for *trans-cis* isomerization in the S<sub>1</sub> state of acetylene.

Information about photolysis transition states comes from the vibrational population distribution of photofragments and from inter-species rotation-vibration *correlated* population distributions. Vibrational satellites on the J=0-1 rotational transition of HCN/HNC in the Chirped-Pulse millimeter-Wave (CPmmW) spectrum reveal the mechanism(s) of 193 nm photolysis of Vinyl Cyanide. Correlated population distributions of CO and H<sub>2</sub>, observed by Velocity Map Imaging (VMI) reveal the roaming mechanism for dissociation of H<sub>2</sub>CO via excitation of selected predissociated levels.

### Introduction

Many spectroscopists view the determination of molecular *structure* as their primary job. But molecules are not static; their dynamical behaviors are encoded in their frequency domain spectra. In isolation and at low internal excitation energy, molecular *dynamics* might appear simple, but the frequency-domain spectrum contains abundant clues about what will happen in collisions and at high excitation energy. Spectra speak to us about *dynamics* in a language that we do not easily or fully understand. We tend to view the extremes of *static geometric structure* and *statistical dynamics* as unrelated (1). However, the intermediate region of *mechanistic dynamics* is rich with encoded insights about dynamical outcomes that *will* happen or *could be made* to happen. Our goal in this chapter is to present examples of ways in which dynamics is encoded in eigenstate-resolved spectra.

Here is a clue. Eigenstates are stationary, but a short-pulse *pluck* of a molecule by electromagnetic radiation can create a coherent superposition of two eigenstates, the dynamics of which is known by the fancy name, *quantum beats* (2). The simple intuitive picture of quantum beats is of a molecule oscillating between two electronic states, one called "dark" and the other "bright." The crucial bit of underlying physics is that two "pure" (zero order) states are "connected" by an *off-diagonal matrix element* of a term in the molecular Hamiltonian (for example, singlet and triplet electronic states interact with each other via the spin-orbit term). The pluck is able to excite both of the two eigenstates (mixtures of the pure bright and dark zero order states) because the bright state character is "shared" between the two eigenstates.

The example of quantum beats sets the stage to understand the ways that many classes of *dynamics are encoded in spectra*. What are the classes of pure states and the physical mechanisms by which these pure states interact? How are these inchoate interactions encoded in spectra? What do we look for? What do we do with them once we have uncovered them? Our job is to decrypt the dynamical code.

### Discussion

### Spectroscopic Perturbations between Two Electronic States of a Diatomic Molecule

Spectra are "assigned" and reduced to tables of multi-digit molecular constants (3) by various forms of pattern-recognition (4–8). Some patterns are so simple that they slap you in the face. Higher-order patterns, albeit simple, are revealed by the use of upper and lower state rotational "combination differences (9)." Highest-order patterns require use of spectroscopic effective

Hamiltonian models (10) to extend assignments when some upper- and lower-state rotational combination differences are unobservable.

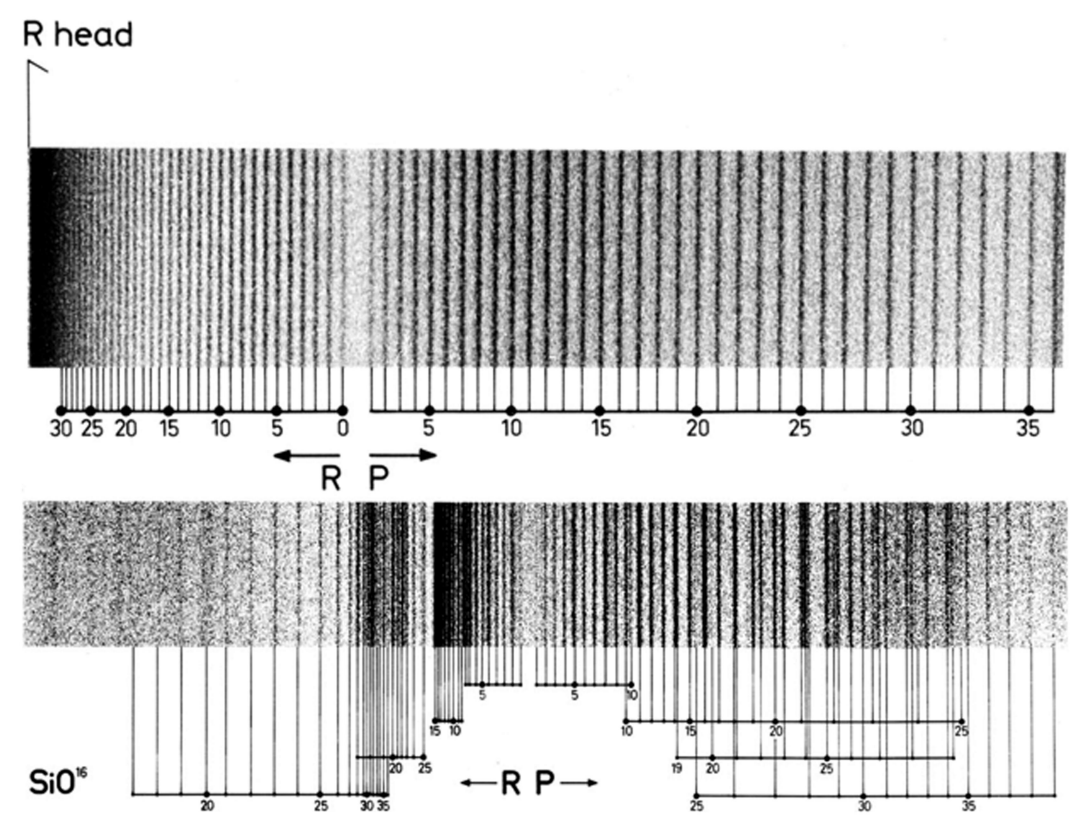


Figure 1. A comparison of the SiO H  $^1\Sigma^+$  (0,0) (top) and (1,0) (bottom) bands. The (0,0) band at 1435 Å is perturbation free, but perturbations in the v=1 level of the H  $^1\Sigma^+$  excited electronic state cause the (1,0) band to be shattered. Only one electronic state is responsible for the disruption of the v=1 level and only one fitted inter-electronic state spin-orbit perturbation matrix element is required to create a fully understood pattern. (Courtesy I.Renhorn) (11). Reproduced with permission from reference (2). Copyright 2004 Elsevier.

Figure 1 shows spectra that sample the v=0 and v=1 levels of the SiO H $^1\Sigma^+$  electronic state (11). The v=0 spectrum defines "simple" and the v=1 spectrum defines "perturbed." A few same-J, same-parity level-crossings of the bright state by a vibrational level of a "dark" state shatters the R and P rotational branches. But rotational assignment is simple, based on perturbation-free lower-state rotational combination differences.

$$R(J-1)-P(J+1) = B''[4J+2]$$

where B'' is the *known* lower state rotational constant, J is the *determined* upper state rotational quantum number, and

$$E(J)' = E_{\nu}(J=0)" + B"(J-1)J + R(J-1)$$

where E(J)' is the energy of the upper state J rotational level, R(J-1) is the energy of the R branch

transition to J' from J''=J'-1, and  $E_{\nu}(J''=0)''$  is the known energy of the lower state  $\nu'', J=0$  level. The key question remains, are these perturbations "one-off" events, or are they the tip of an enormous iceberg of knowledge about electronic structure and dynamics?

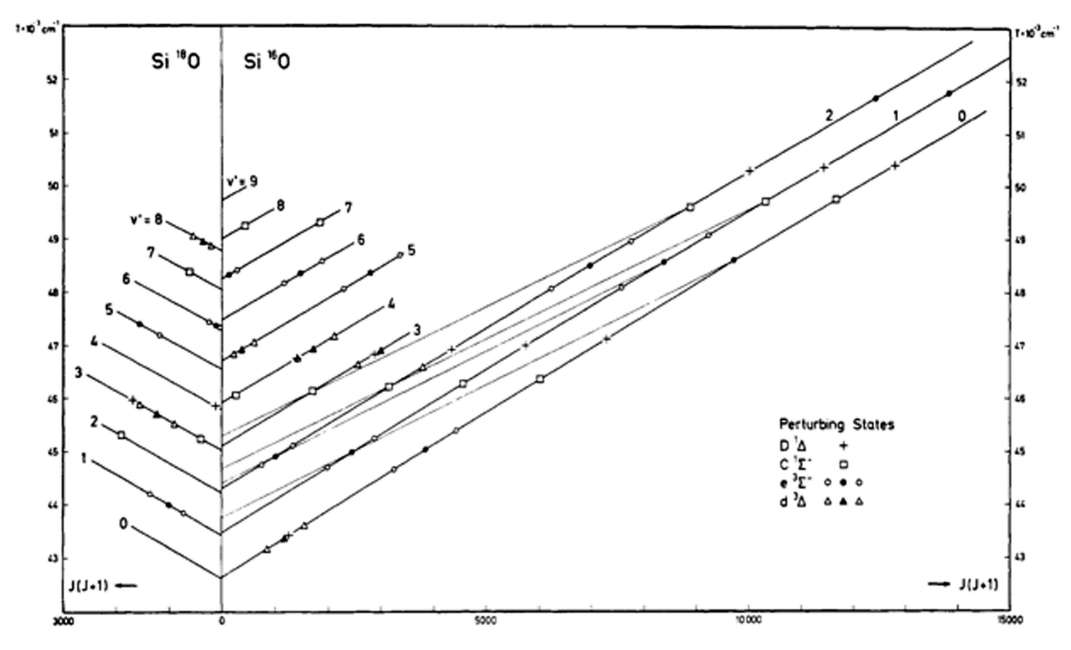


Figure 2. Perturbations in the  $^{28}Si^{18}O$  and  $^{28}Si^{16}O$  A  $^{1}\Pi$  state. The J-values where each A  $^{1}\Pi$  vibrational level crosses a perturber are marked with a different symbol for each observably different type of perturbing state. This sort of collection of multiple perturbation data provides definitive electronic and absolute vibrational assignments of all of the significant perturbers of a chosen spectroscopic "bright state," in this case the A  $^{1}\Pi$  excited state, viewed in absorption from the  $X^{1}\Sigma^{+}$  electronic ground state. Reproduced with permission from reference (15). Copyright 1976 IOP.

The answer to this question should be well anticipated by the reader. There will be many observable perturbations, broken patterns, of several vibrational levels of a well-studied "bright" electronic state. These broken patterns can be sorted into several classes of patterns of broken patterns. (i) The pattern of perturbations between the  $(v_{bright}, v_{dark})$  pair of vibrational levels reveals the electronic symmetry of the dark state (see Kovács, Rotational Structure in the Spectra of Diatomic Molecules, Chapter Four (12)), for example, a <sup>1</sup>\$\Pi\$ state will be perturbed at three closely-spaced rotational levels by  ${}^3\Sigma^+$  or  ${}^3\Sigma^-$  states, for  ${}^3\Sigma^+$  the perturbations occur twice in the f-symmetry component and once at an in-between *I*-value in the e-symmetry component and, for  ${}^{3}\Sigma^{-}$ , twice in e-symmetry and once in f-symmetry. (ii) There will be a series of perturbations of vibrational levels of a single bright electronic state by several vibrational levels of a single dark electronic state, the perturbation matrix elements will exhibit a pattern of magnitudes given by the product of a vibration-independent electronic factor and a calculable, vibration-dependent vibrational factor, from which the "matrix element method (13, 14)" reveals the absolute vibrational numbering of the dark state perturbers (15) (as shown in Figure 2). (iii) The *J*-dependence of the perturbation matrix element reveals whether the interaction is homogeneous ( $\Delta\Omega$ =0, J-independent matrix element), or heterogeneous ( $|\Delta\Omega|$ =1, J-dependent matrix element). (iv) The electronic factor of the perturbation

matrix element may be reduced to a one-electron spin-orbit or L-uncoupling matrix element or a two-electron inter-electron repulsion,  $1/r_{ij}$ , matrix element. (v) The value of the perturbation matrix element, determined from accurately measured (one part in  $10^6$ ) energy levels rather than poorly measured (one part in 10) relative intensities, enables accurate predictions of J-dependent dark-state radiative lifetimes (and relative intensities of transitions) and magnetic g-values (16). (vi) the eigenvectors of the perturbation Hamiltonian contain a complete set of bright~dark mixing coefficients, which provide a predictive map of the most facile inter-electronic state collision-induced energy transfer pathways: the "energy transfer superhighways (17)."

### Anharmonic Interactions among Vibrational Modes of a Polyatomic Molecule: Polyads

An N-atom polyatomic molecule has 3N-6 vibrational normal modes. Perturbations due to anharmonic interactions between vibrational states will be numerous. Some arise from accidents of near-degeneracy, but many are *accidents on purpose*. Whenever a molecule contains two chemically identical A-B bonds or ABC bond angles, there will be symmetric and antisymmetric vibrational *normal modes* of similar frequencies. This results in the occurrence of dynamically important 2:2 "Darling-Dennison" anharmonic resonances via the  $k_{sym-anti}Q_{sym}^2Q_{anti}^2$  anharmonic term, for which the off-diagonal matrix elements between systematically near-degenerate vibrational levels,

$$< v_{\text{sym}}, v_{\text{anti}} | k_{\text{sym-anti}} Q_{\text{sym}}^2 Q_{\text{anti}}^2 | v_{\text{sym}} \pm 2, v_{\text{anti}} \mp 2 >$$

scale approximately proportional to  $v_{\text{sym}}v_{\text{anti}}$  (18). The nonzero matrix elements of the Darling-Dennison term follow the selection rules  $\Delta v_{\text{sym}} = \pm 2.0$ ,  $\Delta v_{\text{anti}} = \mp 2.0$ . As excitation energy increases, the *magnitudes* of the coupling matrix elements and the *number* of quasi-degenerate vibrational basis states increase. For example, when  $v_{\text{sym}} + v_{\text{anti}} = 10$  there are 6 totally symmetric basis states ( $v_{\text{sym}}$ ,  $v_{\text{anti}}$ ) = (10,0), (8,2), (6,4), (4,6), (2,8), and (0,10) and 5 nontotally symmetric basis states (9,1), (7,3), (5,5), (3,5), and (1,9). The totally symmetric interaction matrix elements are proportional to 13.4, 25.9, 31.0, 25.9, and 13.4 and the nontotally symmetric matrix elements are proportional to 20.8, 29.0, 29.0, and 20.8. In contrast, there are only two interacting basis states for  $v_{\text{sym}} + v_{\text{anti}} = 2$ , and the (2,0)~(0,2) interaction matrix element is proportional to 2.0. The matrix that describes the coupled near-degenerate basis states is called a *polyad*, the *polyad number* is  $N=v_{\text{sym}}+v_{\text{anti}}$ , the average value of the intra-polyad matrix element increases roughly as  $(N/2)^2$ , and the eigenvectors approach *local-mode* character at high excitation energy, especially near the middle of the polyad (18–23).

Local modes are special because, at large-amplitude excitation, they typically follow a minimum energy path toward an isomerization transition state (23). Polyads, owing to the increase in both matrix element size and the number of mutually interacting members as the polyad number increases (18–24), are much more robust than normal mode product states. At chemically relevant excitation energies, state space can be dominated by Darling-Dennison polyads (18, 25). Most of these high energy polyads are built on top of a small number of quanta of the highest frequency non-polyad normal modes. This is dynamically significant because the quanta in the normal modes that are not explicitly involved in a Darling-Dennison interaction are not supposed to affect the numerical values of the matrix elements in the set of N to N+1 self-replicating polyad matrices (10). The pattern of broken patterns defined by a family of polyads will break when the large amplitude local mode

motion, in combination with excitation in a non-polyad promoting mode, leads to a close approach to an isomerization transition state (26).

Polyads are a pattern of broken patterns. They are ubiquitous and of obvious dynamical significance. At energies far above where the normal mode picture fails utterly, polyads provide a compact numerical description, physical insight, and a template for rational external control of vibrational dynamics. Eigenvector character, transition relative intensities, and a mechanistic explanation for the small number of "magic" eigenstates that have unexpected chemical properties flow from the polyad model. But the polyad model must break at the energy and state space location of an isomerization transition state (26). This broken pattern of broken patterns appears because the normal mode language spoken by one isomer is different, like English to German, from that spoken by the other isomer. There are many similarities (some of the same normal modes for both isomers), but the similarities are embedded in so many unfamiliarities (totally unrelated normal modes) that the message cannot be decoded.

We have arrived at the threshold of the penultimate step of our journey. This broken pattern of broken patterns is capable of revealing the energy and vibrational shape/structure of a transition state!

### Polyads in the S<sub>0</sub> and S<sub>1</sub> States of Acetylene

The  $\widetilde{X}^{1}\Sigma_{g}^{+}$  (S<sub>0</sub>) state of acetylene is linear. It has seven vibrational normal mode degrees of freedom, two doubly degenerate bending modes,  $\pi_g$  (trans bend) and  $\pi_u$  (cis bend), modes-4 and -5, and three stretching modes,  $\sigma_g$  (symmetric C-H stretch),  $\sigma_g$  (C-C stretch), and  $\sigma_u$  (anti-symmetric C-H stretch), modes-1, -2, and -3. The frequencies of these modes are in the approximate ratios 5:3:5:1:1 (19). Kellman showed that, in addition to the rigorously conserved g/u symmetry, there are four approximately conserved polyad quantum numbers,  $N_{\text{stretch}} = v_1 + v_2 + v_3$ ,  $N_{\text{bend}} = v_4 + v_5$ ,  $N_{\text{resonance}} = 5v_1 + 3v_2 + 5v_3 + v_4 + v_5$ ,  $\ell_{\text{total}} = \ell_4 + \ell_5$  (24). These quantum numbers are approximately conserved despite the effects of the strongest anharmonic interactions among these modes. In the absence of collisions, these polyad quantum numbers are well conserved (until the polyads start to break). However, the  $\ell_{
m total}$  quantum number should be especially vulnerable to collisional relaxation. In particular, polyads with the same values of  $(N_{stretch}, N_{bend}, N_{resonance})$  but values of  $\ell_{total}$ different by an even integer will contain sub-sets of eigenstates with nearly identical energies. Interpolyad collisional transfer among these quasi-degenerate sets of eigenstates will be facile. This is a prediction, not an observation. Polyads, each consisting of many mutually interacting normal mode basis states, are labeled by  $[N_{\text{stretch}}, N_{\text{bend}}, N_{\text{resonance}}, \ell_{\text{total}}, g/u]$ . The vibrational Hamiltonian is block-diagonal in polyad blocks. Polyad membership and the magnitudes of intra-polyad matrix elements are governed by the selection rules and quantum number scaling rules of the harmonic oscillator displacement and vibrational angular momentum operators  $Q_1$ ,  $Q_2$ ,  $Q_3$ ,  $Q_4$ ,  $\ell_4$ ,  $\ell_5$ , and  $\ell_5$  (10).

Polyads are vastly more robust than normal modes. As vibrational excitation energy increases, the number and strengths of inter-mode anharmonic interaction matrix elements increase rapidly. It might seem that ergodicity is taking over and wiping out any sort of mechanistic balls-and-springs picture. But this is not true. Once one example of an anharmonic interaction, for example the stretch or bend Darling-Dennison  $k_{1133}\mathbf{Q_1}^2\mathbf{Q_3}^2$  or  $k_{4455}\mathbf{Q_4}^2\mathbf{Q_5}^2$  interaction, is observed at low excitation energy, the interaction matrix element may be determined via a local, quasi-degenerate state

deperturbation fit model. Then *all examples* of this interaction at higher vibrational excitation energy can be accurately accounted for by matrix element vibrational quantum number scaling rules. The onset of ergodicity is only apparent! As the vibrational excitation energy increases, the polyad blocks in the vibrational effective Hamiltonian get larger and larger, but all of the vibration-rotation eigenvalues and eigenvectors remain accurately predictable. This is a **pattern of broken patterns.** 

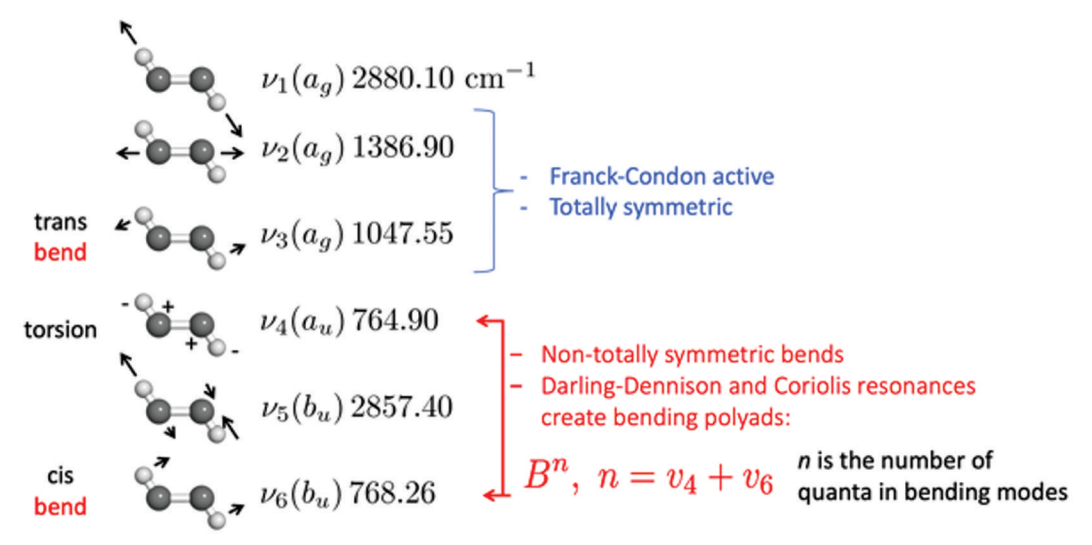


Figure 3. Normal modes of the HCCH  $S_1$  trans-bent conformer. The displacement structure, mode-#, symmetry, and frequency of the 6 normal modes are presented. Modes 2 and 3 are Franck-Condon active from the linear  $S_0$  electronic ground state. Modes 4 (torsion,  $a_u$ ) and 6 ("cis-bend,"  $b_u$ ) have nearly identical frequencies and are strongly mixed by both a Darling-Dennison 2:2 anharmonic interaction and a Coriolis interaction. The result is the domination of state-space by bending polyads, denoted by  $B^n$ , where  $n=v_4+v_6$ . The anharmonic interaction between modes 3 (trans-bend) and 6 (cis-bend) is needed to create a local-bender, but the strong interaction between the normal modes with frequencies 1047.55 and 768.26 cm<sup>-1</sup> is frustrated and apparently concealed by the strong mixing between modes 4 and 6. Adapted with permission from reference (26). Copyright 2015 AAAS.

What does this buy us? It documents the emergence of local modes, the mechanisms for fastest intramolecular dynamics, the information needed to compute relative transition intensities and to extrapolate to the expected level structure and eigenvector characters anywhere within highly excited state space, the XCC method to disentangle overlapping polyad patterns, conversion of a quantum mechanical representation into a classical mechanical map of classical phase space, a basis for rational control of intramolecular dynamics, and a guide to detection of and access to a transition state via a broken pattern of broken patterns.

As the vibrational excitation energy increases, each polyad expands both in number of states and spectral extent. The polyads overlap and it becomes difficult to disentangle them. However, a pattern-recognition technique (discussed below) enables experimental observation of the polyad-by-polyad patterns in a spectrum. An N-transition pattern consists of N-1 adjacent-level energy spacings and N-1 relative intensities. This is a lot of information! Disentangled polyad patterns are observable by cross-correlation of two (or more) dispersed fluorescence spectra that originate from different assigned vibrational levels of an electronically excited state (6).

For example, in the fluorescence spectrum of the bent-to-linear  $\widetilde{A} \to \widetilde{X}$  electronic transition of acetylene, the *trans*-bending vibration (mode-4 in the  $\widetilde{X}$  state, mode-3 in the  $\widetilde{A}$  state) is strongly Franck-Condon active and the C-C stretch (mode-2 in both states) is less strongly Franck-Condon active (see Figure 3). Using a tunable laser to excite from the v''=0 level of the linear  $\widetilde{X}$  state, one can excite to an assigned, low-J' state of, for example, the  $v_3'=2$  and 4 levels of the *trans*-bending mode of the trans-bent  $\widetilde{A}$  state. The energy difference of the  $(v_3',K',J')=(2,1,1)$  and (4,1,1) eigenstates,  $E'_{4,1,1}-E'_{2,1,1}$ , is directly observed in the tunable laser excitation spectrum, hence is precisely known. The  $\widetilde{X}$  state polyads have a convenient structure in which the total intensity in the  $[N_{\text{stretch}}=0,N_{\text{bend}}=v_4'',N_{\text{resonance}}=v_4'',\ell_{\text{total}}''=0$  and 2, gerade] polyad derives from a single bright state, the  $\widetilde{X}$   $(v_1''=0,v_2''=0,v_3''=0,v_4''\neq0,l_4''=0$  and  $2,v_5''=0,l_5''=0$ ) trans-bending overtone basis state.

### Recovery of Patterns: Extended Spectral Cross-Correlation (XCC) Method

The energy level pattern within each polyad is *experimentally revealed* by the Extended Spectral Cross-Correlation method (6). **Two** (or more) dispersed fluorescence spectra are recorded from known and assigned low vibration-rotation levels of the  $\tilde{A}$  state: for example, the  $(v_3',K',J')=(2,1,1)$  and (4,1,1) levels. The (4,1,1) dispersed fluorescence spectrum is shifted by  $E'_{4,1,1}-E'_{2,1,1}$  to bring the lower-state energy levels in its spectrum to the same energies as those in the (2,1,1) spectrum. Both spectra will contain transitions into levels of the

[
$$N_{\text{stretch}}=0$$
,  $N_{\text{bend}}=v_4$ ",  $N_{\text{resonance}}=v_4$ ",  $\ell_{\text{total}}=0$  and 2,  $gerade$ ]

polyads intermingled with levels that belong to other polyads. A *recursion map* reveals the polyad pattern freed from overlapping other-polyad transitions (6).

A 2-dimensional recursion map is constructed by dividing each of the two dispersed fluorescence spectra into "resolution elements" and measuring the integrated intensity in each resolution element,  $\{I_i\}$ . These resolution elements might correspond to  $\sim 1/2$  of the chosen spectrograph resolution of the dispersed fluorescence spectrum, say 2 cm<sup>-1</sup>. If the spectrum covers 2000 cm<sup>-1</sup> there are 1000 resolution elements. Each of the 1000 points on the recursion map is plotted as the intensity for the i<sup>th</sup> resolution element of spectrum 1,  $I_i(1)$ , vs. the corresponding quantity from spectrum 2,  $I_i(2)$ . The plot consists of 1000  $[I_i(1), I_i(2)]$  points. Note that the recursion map itself contains no information about the energy of each of the resolution elements. Figure 4 is an example of how such a recursion map is constructed and used.

The dimension of each polyad can be quite large.

[
$$N_{\text{stretch}}=0$$
,  $N_{\text{bend}}=v_4$ ",  $N_{\text{resonance}}=v_4$ ",  $\ell_{\text{total}}=0$ ,  $g$ ]

The polyad contains basis states

$$|v_1,v_2,v_3,v_4,\ell_4,v_5,\ell_5\rangle = |0,0,0,v_4|,0,0,0\rangle, |0,0,0,v_4|-2,0,2,0\rangle, ... |0,0,0,0,0,v_4|,0\rangle,$$

$$|0,0,0,v_4|-2,2,2,-2\rangle, ... |0,0,0,2,2,v_4|-2,-2\rangle, |0,0,0,v_4|-2,-2,2,2\rangle, ... |0,0,0,2,-2,v_4|-2,2\rangle,$$

in addition to basis states with  $|\ell_4|$  and  $|\ell_5| > 2$ . If, for example,  $v_4'' = 10$ , this list contains 6+4+4=14 basis states. The  $[0, v_4'', v_4'', 2, g]$  polyad, which is also accessed from the  $|v_3', J=1, K'=1>$  eigenstate of

the  $\tilde{A}$ -state, is constructed from a similar number of  $\tilde{X}$ -state basis states as the  $[0,v_4",v_4",2,g]$  polyad. Polyads with  $N_{\text{stretch}}>0$ ,  $\ell>2$ , or with *ungerade* symmetry can be observed via hot-band or IR-UV double resonance excitation into a chosen, securely assigned, vibration-rotation level of the  $\tilde{A}$ -state (24).

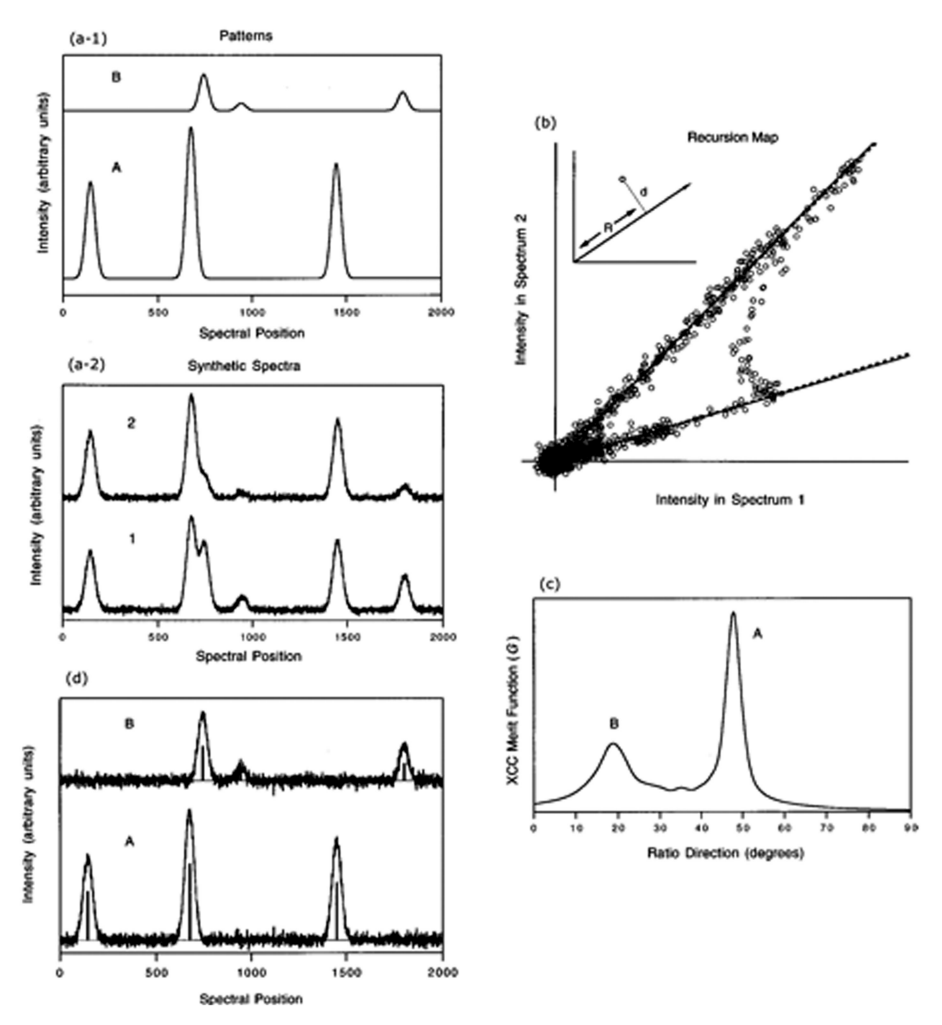


Figure 4. Extended cross correlation (XCC). (a-1) Patterns A and B both appear, with different relative intensities in Spectra 1 and 2. (a-2) Noise is added to the two spectra; (b) the Recursion Map is a plot, resolution element by resolution element, of the intensities in Spectrum 1 vs. the intensities in Spectrum 2. The two straight lines from the origin represent patterns A and B. The slopes of the two lines are the ratios of patterns A and B in spectra 1 and 2. The inset shows how the intensity of each point in each spectrum is related to the fitted ratio direction (R) and the perpendicular offset (d) from this ratio direction. (c) The XCC merit function comes from a robust estimator fit of the angles that best describe each ratio direction. (d) Patterns A and B are reconstructed, based on the two ratio directions determined on the merit function plot, by apportioning the intensity in each resolution element to patterns A and B. Adapted with permission from reference (6). Copyright 1997 AIP Publishing.

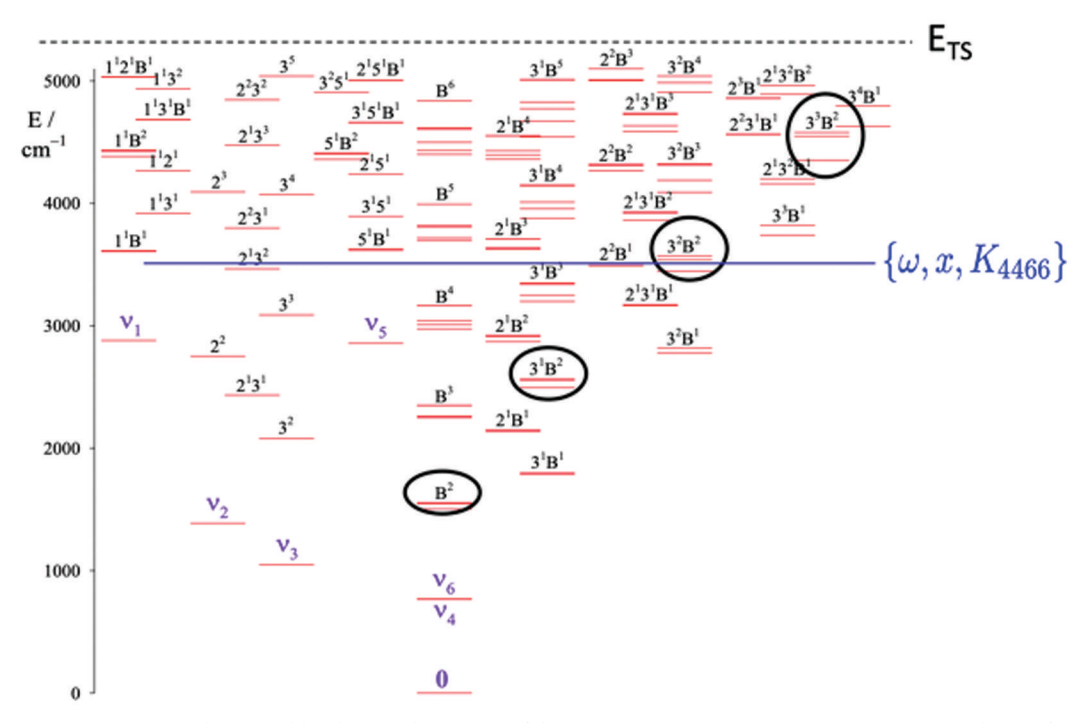


Figure 5. Every vibrational level up to the energy of the trans-cis isomerization transition state is observed, assigned, and fitted. Notice the frequent appearance of the polyad symbol, B<sup>n</sup>. State space is dominated by mode-4~mode-6 bending polyads. The interactions and basis-state membership in all of these polyads are inter-related. The H<sup>eff</sup> polyad fit model generates an eigenvector for every eigenstate. A series of polyads built on 0, 1, 2, and 3 quanta of mode-3 are labeled by enclosure in an oval. Although the polyad model is supposed to be unaffected by quanta in a non-polyad mode, a breaking of the polyad pattern of broken patterns reveals the energy and structure of the trans-cis transition state. Adapted with permission from reference (25). Copyright 2011 AIP Publishing.

A recursion map (see Figure 4) constructed from two spectra, spectrum 1 and spectrum 2, that contain transitions that belong to two polyads, polyad A and polyad B, (as well as other unrelated transitions), will display points clustered along two straight lines that originate from 0,0  $[I_i(1)=0, I_i(2)=0]$  in addition to scattered points, which are especially numerous near 0,0. Each point expresses the intensity in the i<sup>th</sup> resolution element of spectra 1 and 2. The transition frequencies of these i resolution elements do not appear on the recursion map itself, but the transition frequency of each resolution element is taken from the resolution elements of the original spectra:  $\{I_i(1) \text{ and } I_i(2); i=1 \text{ to } i_{max}\}$ . Each straight line is associated with one of the polyad patterns. Separated polyad patterns A and B are reconstructed from the subset of  $I_i(1), I_i(2)$  points clustered along one of the straight lines on the recursion map.

Dispersed Fluorescence spectroscopy, using a 1-meter monochromator equipped with an intensified 2-D CCD detector, is a convenient but low-resolution technique for the systematic study of the polyads in the acetylene  $\widetilde{X}$ -state. Since accurate *relative intensities* are an essential requirement for the success of XCC, *high resolution* two-laser schemes (Stimulated Emission Pumping (27–29) and Four Wave Mixing (30)) could not be used. XCC reveals "feature states" within each polyad rather than eigenstates. Feature states are sufficient to capture the big picture of intramolecular

dynamics in vibrationally highly excited acetylene. One of the most important features revealed in Dispersed Fluorescence (31, 32) and SEP experiments is the emergence of large amplitude local-bender eigenstates (23, 24). In most molecules, the minimum energy path to an isomerization transition state involves *one large amplitude local mode motion*. On the electronic ground state potential surface of acetylene, the local bend is along the path toward vinylidene (23).

One of the authors of this paper was a member of the Klemperer research group. Whether Klemperer believed it or not, we liked to say that Klemperer's first rule is that a low-resolution spectrum is always misassigned. The XCC method provides assignments of "feature states" rather than eigenstates. At high vibrational excitation, feature state assignments are more dynamically relevant and robust than those of eigenstates.

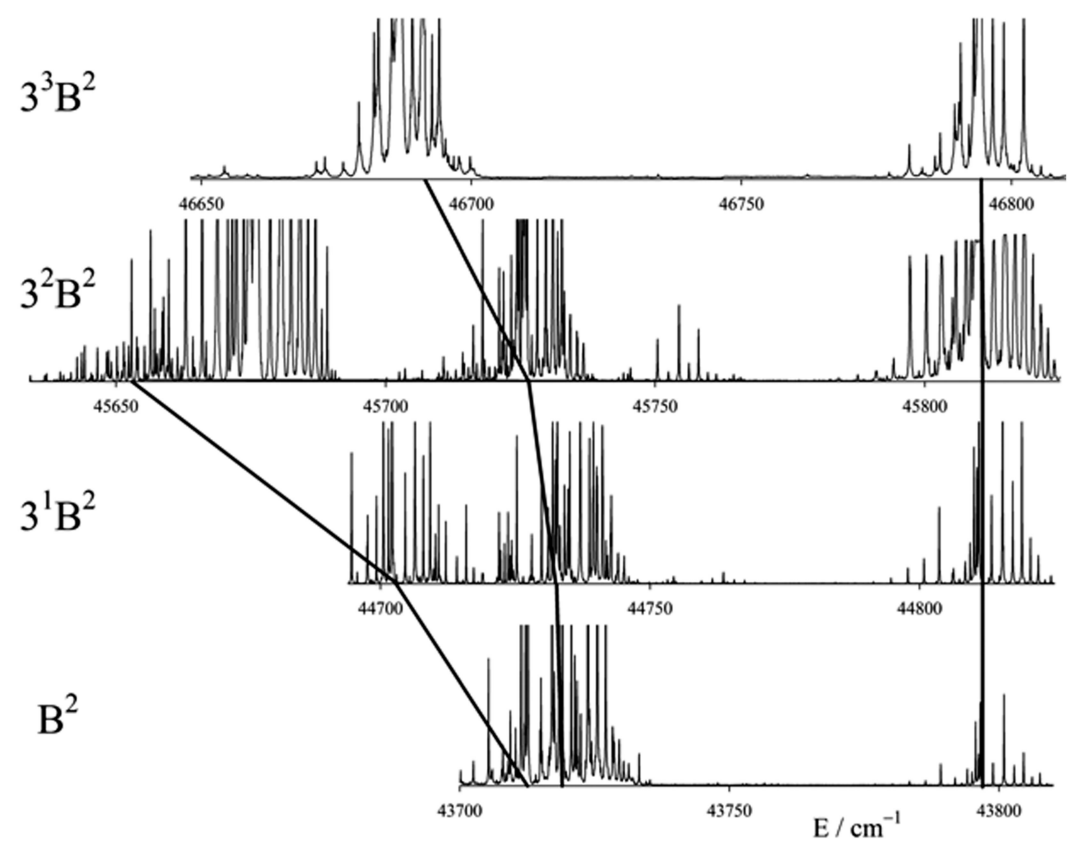


Figure 6. Excitation in  $\nu_3$  shatters the  $(\nu_4, \nu_6)$  bending polyads. The spectra shown are the K'=1 sub-bands of the  $3^nB^2$ , n=0-3 polyads. The spectra are arranged so that the highest frequency sub-bands (nominally  $3^n4^2$  are aligned vertically. It appears that the addition of quanta in mode-3 causes a small but slowly increasing lower frequency shift of the nominal  $3^n4^16^1$  sub-band and a large and rapidly increasing shift of the nominal  $3^n6^2$  sub-band. This is not supposed to happen. Crucial information about the energy and structure of the trans-cis isomerization transition state is provided by how excitation in mode-3 causes the structure of the  $(\nu_4, \nu_6)$  bending polyad to break. Detailed analysis shows that the isomerization is in-plane, not torsional, and that mode-4 plays a spectator role. Reproduced with permission from reference (33). Copyright 2009 Elsevier.

Order-of-magnitude advances in experiment and data processing are making it possible to ask and answer questions that had been unimaginable. XCC is the analysis method that exploits an experimental capability to record simultaneously many transition frequencies *and* intensities. Multiplexed and correlated data acquisition are capable of pulling back the curtain of apparent complexity to reveal mechanisms of molecular dynamics that are causal rather than statistical and based on a localized event rather than a quantum mechanical integral over all space. Polyads are robust. They are a conceptual tool that extends insight and understanding to real molecules at work rather than toy models at play.

Polyads are an example of a pattern of broken patterns. The XCC method demonstrates, in principle, that spectrally overlapping polyads can be disentangled. Polyads are self-replicating patterns. The lowest energy member of a family of polyads can be examined at high resolution free of overlap with other polyads. Once this is accomplished, we know the names of the interacting basis states and the values of the relevant interaction matrix elements and deperturbed vibration-rotation constants are determined by a few-states deperturbation analysis. The XCC method permits extension of the polyad representation to higher energy where the polyad matrices are large and multiple polyads overlap. The polyads serve as a map of state space which can guide the experimentalists (and theorists) along a path toward an isomerization transition state. The polyads encode information about the energy and structure of the transition state. This information is encoded in the ways that the polyad structure breaks! We encounter and exploit a **broken pattern of broken patterns**.

#### A Broken Pattern of Broken Patterns

When a pattern breaks, far from being a loss that one mourns, it is an opportunity to view territory deemed intractable by textbooks. The transition state is a central concept of Chemistry. A chemical system spends only a few femtoseconds (half of a vibrational period) traversing a transition state. How can high resolution *frequency domain* spectroscopy tell us anything about a transition state? We know that the polyad model can generate the large amplitude local motions that map the approach to a transition state. How do spectrally resolved (0.1 cm<sup>-1</sup> FWHM) and assigned eigenstates encode few femtosecond transit through the transition state? The time-energy uncertainty principle rings the alarm bells: 5 fs  $\leftrightarrow$  2000 cm<sup>-1</sup> vs. 0.1 cm<sup>-1</sup> $\leftrightarrow$  100 ps. The  $\sim$ 5 fs dynamical information is encoded in a  $\sim$ 2000 cm<sup>-1</sup> wide region of the spectrum that contains many spectral lines from multiple overlapping polyads. A very small fraction of these spectral lines belongs to broken polyads. The code is written in specific (and *a priori* specifiable) polyads. Which polyads? How are they broken? The polyads in the energy region of the *trans-cis* isomerization barrier in the acetylene S<sub>1</sub> state have a beautiful story to tell.

### Polyads Encode trans-cis Isomerization on the Acetylene $S_1$ ( $\widetilde{A}^1A_u$ ) Potential Surface

The  $S_1$  ( $\tilde{A}^1A_u$ ) electronic state of acetylene has a planar trans-bent structure. There are six vibrational modes (34):

mode symmetry description frequency/cm <sup>-1</sup>						
1	$a_g$	symmetric C-H stretch	2880.0	8		
2	$a_g$	C-C stretch	1386.9	0		
3	$a_g$	in-plane trans-bend	1047.55			
4	$a_u$	torsion (out of plane bend)		764.90		
5	$b_{u}$	antisymmetric C-H stretch		2857.4		
6	6 b <sub>u</sub> antisymmetric in plane bend (" <i>cis-</i> bend")		768.26			

Every vibrational level of the trans-bent conformer (and several levels of the cis-bent conformer) has been observed, assigned, and fitted, from the v=0 level ( $T_0$ =42197.7 cm $^{-1}$ ) up to energies above the H +CCH dissociation limit (46074 cm $^{-1}$ ) and the computed energy of the isomerization barrier ( $T_e(\tilde{A}^1A_u)$  + 4979 cm $^{-1}$ ). The frequencies of modes-1 and -5 and of modes-4 and -6 are nearly identical and are subject to 2:2 Darling-Dennison anharmonic interactions (18). The low and matching frequencies of modes-4 and -6 result in state space being dominated by  $v_4$ , $v_6$  polyads, especially  $B^n$  (n= $v_4$ + $v_6$ ) polyads built on quanta of the Franck-Condon active mode-3, in particular the singularly important  $B^2$ ,  $3^1B^2$ ,  $3^2B^2$ ,  $3^3B^2$  series of polyads. The energies and assignments of all of the vibrational levels of the *trans*-bent isomer are shown in Figure 5. Figure 6 and Table 1 show how the structure of the  $B^2$  polyad is strongly affected by quanta in mode-3, which might have been expected to be a "spectator" mode. The  $B^2$  polyad consists of three basis states:  $4^2$ ,  $4^16^1$ , and  $6^2$ . It appears that the  $B^2$  polyad built on 0, 1, 2, and 3 quanta of mode-3 is primarily distorted by a much larger shift of the  $6^2$  than the  $4^2$  level. Why? Because modes-3 and -6 are symmetric and antisymmetric in-plane bending levels. They want to mix in order to produce in-plane local-bender progeny. Mode-4 acts as a spectator and mode-3 acts as a "promoter."

Table 1. Numerical Example of Polyad Breakdowna

	$B^2$	$B^3$
$\nu_3 = 0$	-51.678*	-51.019*
$\nu_3 = 1$	-60.101	-57.865
$\nu_3 = 2$	-66.502	

<sup>&</sup>lt;sup>a</sup> Adapted from polyad fits reported in reference (33).

In Table 1, the vibration dependence of the polyad is described by the quantum number scaling rules of the  $K_{4466}Q_4^2Q_6^2$  anharmonic interaction term. The fitted value of  $K_{4466}$  is supposed to be independent of  $\nu_3$ , but it clearly is not.

cis-trans isomerization across a C=C double bond usually involves torsion rather than in-plane motion (35, 36). However, on the  $S_1$  potential surface of acetylene, the lowest energy isomerization transition state involves the in-plane rather than torsional path. Experimentally, the isomerization path is encoded in the mode-3 distortion of  $B^n$  polyads. Theoretical calculations agree with the experimental determination of the energy of the isomerization barrier and the planar, near half-linear

shape of the transition state. The key point is that only a small fraction of the eigenstates in the energy region of the transition state are proximal to the isomerization path. "Proximal" means that the  $3^mB^2$  wavefunctions have significant overlap with the minimum energy isomerization path.

Textbook authors (37), in making their claim that a transition state could not be directly sampled by frequency domain spectroscopy, failed to consider that the isomerization barrier is located at an energy region in which eigenstates are discrete and in which only a small fraction of those eigenstates correspond to wavefunctions that are proximal to the isomerization path. Information about the location and structure of the transition state is encoded in a pattern of assigned and polyad model fitted eigenstates. This pattern would be unrecognizable if one were to apply statistical measures to all of the eigenstates in the absence of polyad model assignments.

The quantum mechanical polyad model permits determination of effective frequencies for classical mechanical motions along paths in the region of the transition state. The effective frequency along the isomerization path is zero at the top of a barrier. Quantum mechanical states do not sample the barrier region continuously, so they cannot *directly* sample the zero effective frequency region. However, the quantum mechanical polyad model *can be* transformed into an action-angle classical mechanical representation. This representation permits interpolation to the total energy and nuclear configuration point of zero effective frequency on the potential energy surface.

The message here is that it is difficult to recognize a pattern in a dense forest of eigenstates unless you know the nature of the pattern for which you are looking. The emergence of local modes is always going to be important along the minimum energy path toward a transition state.

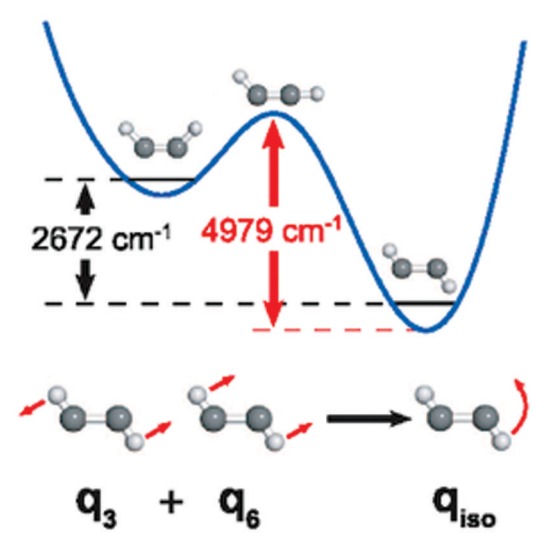


Figure 7. The transition state for trans-cis isomerization on the HCCH  $S_1$  potential surface. Examination of the vibrational structure of  $S_1$  acetylene reveals the energy and structure of the transition state for trans-cis isomerization. The symmetric (mode-3) and antisymmetric (mode-6) bending modes combine to form the local-bender motion, which is along the minimum energy isomerization path. Reproduced with permission from reference (26). Copyright 2015 AAAS.

In the acetylene  $S_1$  state, the Darling-Dennison interaction between a symmetric and an antisymmetric stretch leads to a large amplitude local C-H stretch in the plane of the molecule along an axis roughly  $30^0$  from the C-C bond axis. The lowest energy interaction between modes-

1 (symmetric stretch) and -5 (antisymmetric stretch) is between the  $1^2$  and  $5^2$  basis states, the energies of which lie slightly above the H + CCH dissociation threshold. One might expect that the Fermi interaction between the near degenerate  $1^2$  and  $1^12^2$  basis states (mode-2 is the C-C stretch) would result in a pattern of state-dependent dissociation rates (a similar interaction between  $5^2$  and  $2^25^1$  is symmetry forbidden). The near perfect degeneracy between the Darling-Dennison interacting modes-4 (torsion) and -6 (*cis*-bend) results in a proliferation of  $B^n$  ( $n=v_4+v_6$ ) polyads that dominate state space. These polyads *might* encode motion toward a non-planar isomerization transition state, but *these polyads are broken* by Fermi interaction of  $6^2$  (but not  $4^2$ ) with mode-3 (*trans*-bend). Spectroscopy (26) and theory (38) agree that the torsional barrier to *trans-cis* isomerization lies at much higher energy than the in-plane barrier via a half-linear transition state. The vibrational normal mode structures and frequencies offer hints about where to look in state space for quantitative information about the energy and structure of isomerization transition states. These hints have led to the characterization of the transition state shown in Figure 7.

### Photofragment Vibrational Population Distributions Encode the Transition States of a Photolysis Reaction

The vibrational population distributions (VPDs) of the HCN and HNC photofragments that result from 193 nm photolysis of Vinyl-Cyanide provide information about transition states (39, 40). The photofragments are born at the transition state. Their VPDs are sampled by Chirped Pulse Millimeter Wave Spectroscopy (CPmmW) (41). H/D isotopic substitution of the parent molecule can be used to turn off one of several possibly competing mechanisms. Although this is not discussed here, the frequency of the photolysis laser can be used to sample different photolysis transition states.

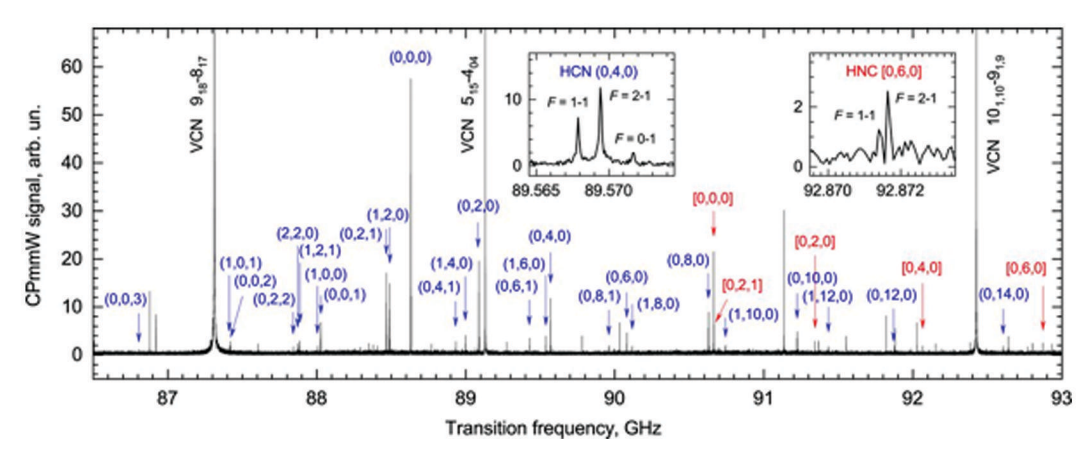
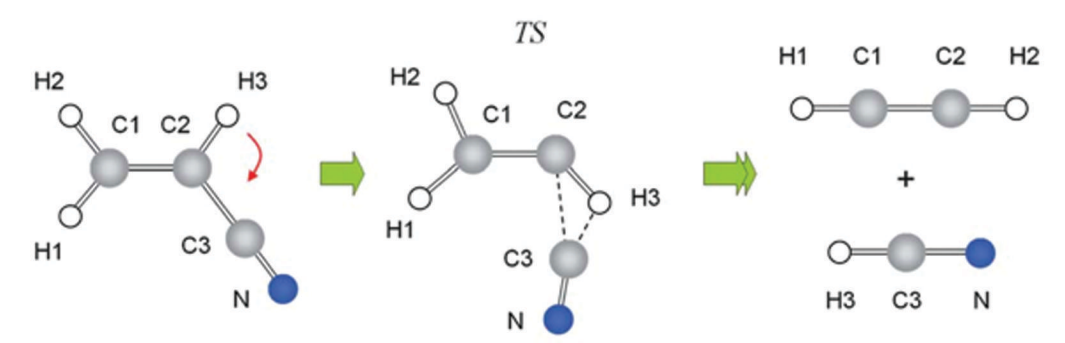


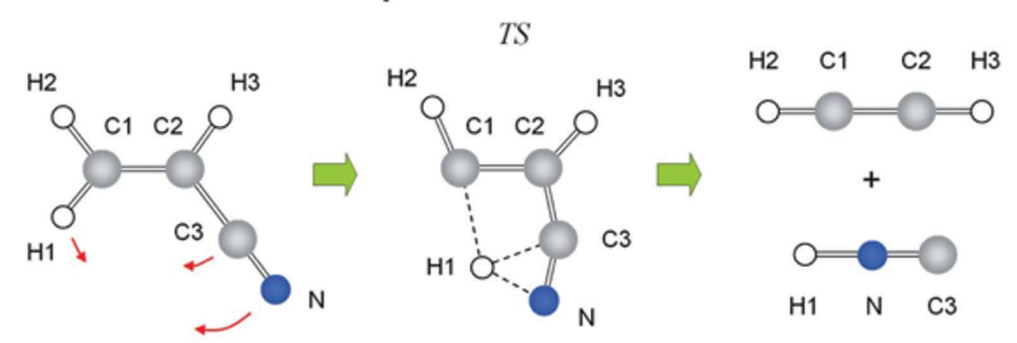
Figure 8. Chirped pulse mm-wave (CPmmW) spectrum of 193 nm photolysis products (HCN and HNC) of vinyl-cyanide. More than 30 assigned vibrational satellites of the J=0-1 rotational transitions of both HCN and HNC. Insets show the distinctly different  $^{14}$ N I=1 quadrupole hyperfine splittings. All of the transitions within the 86.5-93.0 GHz sweep range are sampled in each chirped pulse. Their relative intensities are meaningful and correspond to relative vibrational level populations. Reproduced with permission from reference (39). Copyright 2020 National Academy of Sciences.

The CPmmW spectrum in Figure 8 shows the relative populations of more than 30 assigned vibrational levels of the HCN and HNC photofragments that result from 193 nm photolysis of

Vinyl-Cyanide (VCN). These populations are determined from the relative intensities of "vibrational satellites" of the J=0-1 rotational transition in each vibrational state. This is significant because *all* of these vibrational populations are sampled within *each* frequency chirp over a 6 GHz wide region centered at ~90 GHz, even though the sampled vibrational levels span the 0-10,000 cm<sup>-1</sup> energy region.



## Makes Vinylidene & Local-Bender Acetylene: strong mm-wave transitions ~75 GHz expected.



# Makes *cis*-bending Acetylene: no strong mm-wave transitions expected.

Figure 9. 3-Center vs. 4-center mechanisms for photolysis of vinyl cyanide. This is an over-simplified guesstimate of the mechanisms for the production of HCN and HNC. In the 3-center mechanism the leaving CN group attaches the H3 atom to its C-atom end and departs as HCN. In the 4-center mechanism the leaving CN group attaches the H1 atom to its N-atom end and departs as HNC. The co-product of the 3-center path is vinylidene and from the 4-center path is extreme cis-bending acetylene. Vinylidene has its predicted J=0-1 transition within the chirp range of the CPmmW spectrometer, but this transition was not detected, likely due to collisional relaxation into a dense manifold of highly vibrationally excited acetylene. Reproduced with permission from reference (40). Copyright 2013 Royal Society of Chemistry.

The chirped pulse partially polarizes all two-level systems the frequencies of which lie within the bandwidth of the chirped pulse. Each polarized two-level system relaxes by Free Induction Decay (FID). The FID is an electric field that oscillates at the frequency of the two-level system. *All of the FIDs are detected simultaneously, shot-by-shot.* Detection is multiplexed: 60,000 resolution elements of 100 kHz width are sampled in each shot. More than 100,000 shots (at a repetition rate of 10 Hz) can be phase-coherently averaged. This is an example of a class of experiment that represents a multiple-

order-of-magnitude increase in the quantity and quality of spectroscopic information obtainable. What had seemed impossible has become routine.

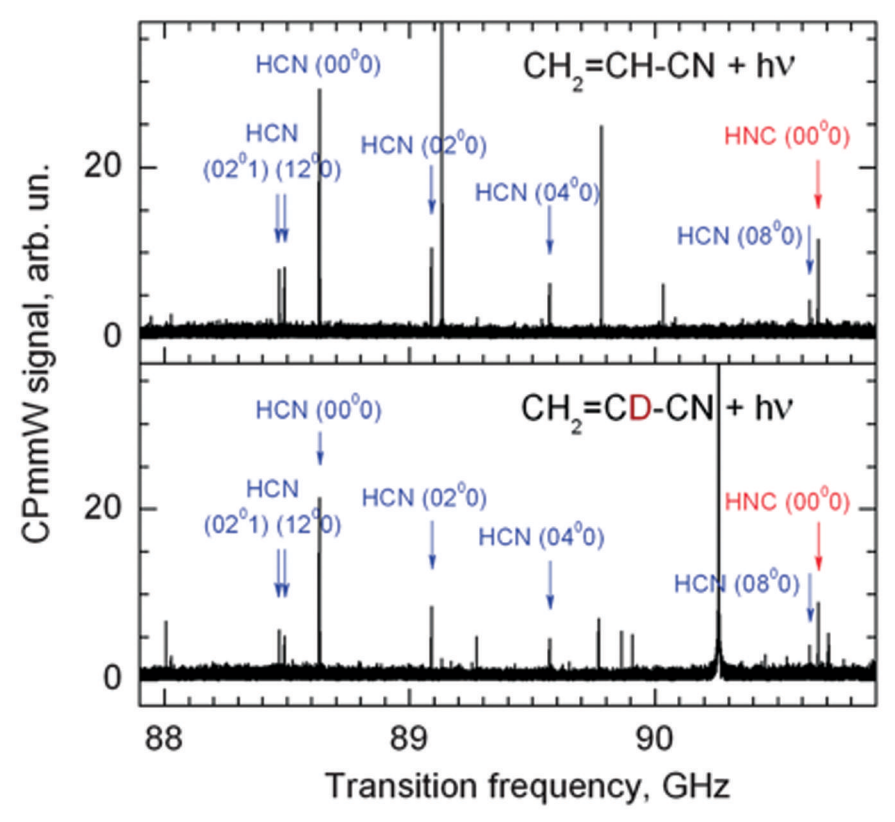


Figure 10. Deuterium substitution should have shut down the 3-center mechanism for the formation of HCN. There are three H atoms in VCN, and each could attach to either end of the CN group. Thus, there are, naively, 6 mechanisms. H/D substitution could shut down the HCN/HNC-forming mechanisms involving the replaced H-atom. Replacing the H3 atom would shut down the 3-center mechanism, which had believed to be dominant. The top and bottom spectra are respectively unsubstituted and H3 replaced by D. Surprisingly, the HCN (0200) and HNC (0000) transitions show only a ~15% decrease in the intensity of the HCN/HNC transitions. Adapted with permission from reference (40). Copyright 2013 Royal Society of Chemistry.

Photolysis of VCN yields HCN or HNC and HCCH or  $CCH_2$  (vinylidene). Three of these possible photofragments have a large permanent electric dipole moment, therefore their pure rotation microwave spectra are, in principle, detectable. Photofragments are formed rotationally hot and must be cooled in a supersonic expansion to ~5 K to optimize the Signal:Noise ratio in the CPmmW spectrum. It is usual to assume that vibrational cooling is much slower than rotational cooling. The VPDs we extract from the spectra are based on assuming that vibrational cooling is negligible. This needs to be the subject of careful experiments as some results suggest efficient vibrational relaxation in collisions between polyatomic molecules (42). No trace of the rotational spectrum of vinylidene has been detected. It seems likely that rotationally hot vinylidene is collisionally transferred in the supersonic expansion into highly vibrationally excited  $S_0$  acetylene. This is too bad for several reasons. Foremost among these: (i) the VPD of vinylidene would provide information about the acetylene-vinylidene transition state on the  $S_0$  potential surface similar to

what was observed for trans-cis isomerization on the acetylene  $S_1$  surface; (ii) motivation would be provided for measurement of correlated product distribution similar to what will be presented in the next section of this paper concerning the correlations observed between the rotation-vibration populations of the  $H_2$  and CO fragments formed by predissociation of  $H_2CO$ . Inter-species correlations represent a new experimental frontier in the characterization of photo-fragmentation mechanisms: the **roaming mechanism**.

Figure 9 illustrates various mechanisms by which HCN or HNC could be formed in the photofragmentation of VCN (40). The first step could involve transfer of the H1 (4-center path) or H3 (3-center path) atom to CN. The H2 atom is likely to be blocked from direct transfer to the exiting CN, however in a roaming type of mechanism the H2 atom could play a role equivalent to that of the H1 atom. One could observe the HCN, HNC VPD that results from nondeuterated VCN, VCN deuterated at H1, at H2, or at H3. One could also observe the DCN, DNC VPD for VCN deuterated at H1, H2, and H3. In this way the contributions to the HCN, HNC VPDs from H1, H2, and H3 could be experimentally separated. Only the effect of H3 substitution was observed, shown in Figure 10. The expectation was that the 3-center mechanism would be the dominant source of HCN, but replacement of H3 by D resulted in the unexpectedly small 15% decrease observed in the total HCN yield. Comparison of the HCN,HNC VPDs to the corresponding DCN,DNC VPDs would reveal post-transfer H (vs. D) between the C- or N-end of the CN. The combination of CPmmW spectroscopy and selective isotope substitution would provide an unprecedentedly detailed picture of the competing mechanisms. But this would still fall short of what could be obtained from interspecies correlated rotation-vibration VPDs.

### **Good News and Bad News**

### Good News

The CPmmW spectrum of the HCN and HNC products of 193 nm photolysis of VCN is an information-rich sample of the photolysis mechanism(s) (39, 40). The multiplexed nature of the experiment makes it possible to obtain a vibrational population distribution from the relative intensities of >30 vibrational satellites of the J=0-1 rotational transition. There is no scanning of the laser and the chirped pulse of the mm-wave radiation samples the complete set of vibrational satellites in the same exact way in every pulse. This is the reason that the observed relative intensities of the vibrational satellite transitions are meaningful. Additional information about the HCN/HNC photolysis products could have been obtained by observing the J=1-2 transition, which simultaneously samples vibrational populations in readily assignable states with both  $\ell=0$  (even- $\nu_2$ ) and 1 (odd- $\nu_2$ ), where  $\ell$  is the vibrational angular momentum associated with  $\nu_2$ , the doubly degenerate bending normal mode. The even-v2:odd-v2 intensity ratio provides information about the planarity of the transition state. There is also the possibility of observing the differences between the VPDs of HCN/HNC and of DCN/DNC that result from replacement of the H by D at each of the three nonequivalent sites in the VCN molecule. H/D isotope substitution permits partitioning the yields of each vibrational level into paths involving abstraction of H or D from each of the three sites.

For photolysis of almost every molecule, the Franck-Condon factors are extremely small for electronic transitions that excite from the electronic ground state v=0 vibrational level of the parent molecule to an energy just above the thermodynamic threshold for photolysis. The result of this Franck-Condon constraint is that excitation must be so far above threshold that multiple fragmentation paths will contribute to the measured VPDs.

For VCN, there are three H atoms and the CN group has two ends. This means that six dissociation continua could be involved. Each of the three H atoms could end up attached to either end of the CN group. How does one extract information about multiple fragmentation pathways from uncorrelated observations of the HCN- and HNC-forming VPDs?

Information about the VPD of the co-fragment (for VCN the co-fragment is acetylene or vinylidene) might be helpful. However, acetylene has zero electric dipole moment hence no pure rotation transition and vinylidene is rapidly transferred by collisions into extremely high vibrational levels of acetylene as the barrier is on the order of 2 kcal/mol (43). The multiplexed capability of the CPmmW scheme is typically applicable to obtaining the VPD of only one of the possible VCN photofragments. But reality is even more unkind. If it were possible to obtain VPDs for more than one co-fragment, each of the single-species VPDs has the same deficiency of a single VPD: the co-fragment VPDs are uncorrelated.

When a molecule is photo-excited to an energy above the thermodynamic threshold for dissociation, it can break into fragments. The simplest class of experiment is to measure the destruction rate of the parent molecule as a function of the frequency (and intensity) of the photolysis radiation. This class of measurement is degraded by imperfect control over the initial internal energy of the parent molecule. The quality of this experiment is enhanced by cooling the internal energy of the molecule to a few Kelvins in a supersonic expansion or in a cryogenic buffer gas cell. Alternatively, photolysis can occur via resonant excitation from a selected parent molecule rotation-vibration level into an assigned rotation-vibration predissociated "level."

Dissociation continua come in many flavors: structureless, lumpy but unassignable, and very sharp with assignable lumps. Predissociated lines are a molecule's gift to the experimentalist, because they report accurately on both the energy above the thermodynamic threshold for dissociation and on the rovibronic quantum numbers of the slowly dissociating parent molecule. Sharp and assignable lumps generally occur near thresholds, but sometimes, *for dynamically special reasons*, such as the need to break two old bonds and form one new bond, dissociation occurs via an assignable "resonance" at an internal energy far above the thermodynamic threshold. However, once dissociation occurs, two fragments are produced, and energy is distributed among the accessible rotation-vibration states of these photofragments. It has become standard experimental procedure to accurately measure the rotation-vibration population distribution of one or both fragments.

The two fragments are born at a transition state, but the information about the energy, structure, and unimolecular dynamics of passage through the transition state is vastly inferior to what might be imagined if it were possible to measure the *correlated* rather than *separate* population distributions of the two fragments. How is the above-dissociation energy distributed between the two fragments that are created in each fragmentation event? What were the inter-fragment impulses and torques as the two fragments separate? Is this separation a single event or a complex progression of interactions and responses? In such a case there might be distinct signatures of the underlying mechanisms in the correlated VPDs.

### **Velocity Map Imaging**

Velocity Map Imaging (44, 45) (VMI) now readily achieves such *quantum state-correlated* measurements: every product in its detected quantum state can be associated state-specifically with its suite of coproducts. This is possible because momentum and energy conservation permit one to infer the total translational energy release between two products based simply on detection of that of one product. Furthermore, VMI allows for very high (velocity) resolution detection of single product quantum states, given as the radii of concentric circles on a position-sensitive detector (46). For photodissociation of small molecules, then, every point in the recovered total translational energy distribution corresponds to some particular internal state of the *undetected* product in a manner somewhat analogous to photoelectron spectroscopy.

These product state correlations convey a detailed accounting of the energy and angular momentum disposal, and, when obtained for a predissociating system in which the parent quantum state is well-defined, afford unique dynamical insights. In studies of predissociation into multiple continua in formaldehyde (47), state-correlated measurements between CO and H<sub>2</sub> revealed surprising interactions among these decay pathways—the roaming radical mechanism —and this has greatly impacted our thinking about the dynamical behavior of reactive systems (48). The discovery of roaming illustrates the power of multiplexed, multiply-resonant preparation and interrogation of an excited system as it decays to products, with quantum number labels at every step.

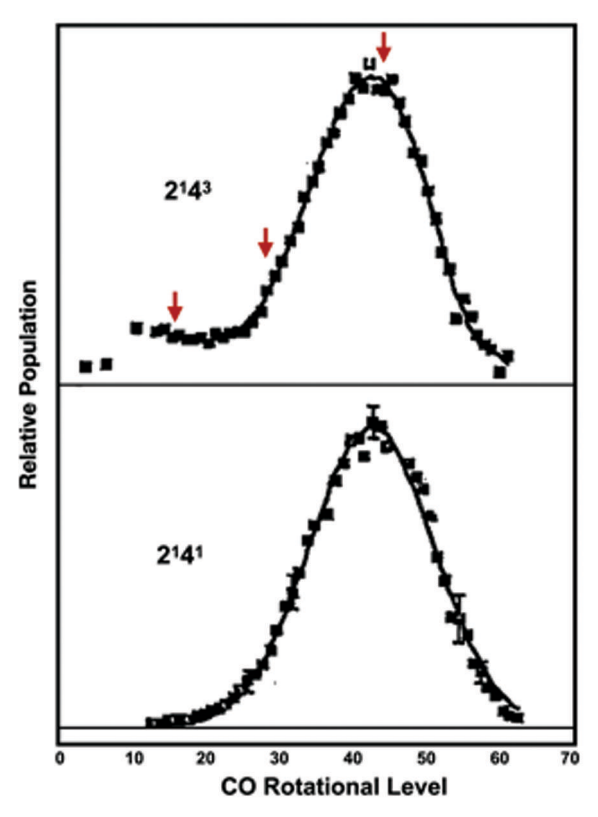


Figure 11. CO (v=0) rotational distributions following photodissociation of formaldehyde at energies just above (top) and just below (bottom) the radical threshold. Adapted with permission from reference (52). Copyright 1993 AIP Publishing.

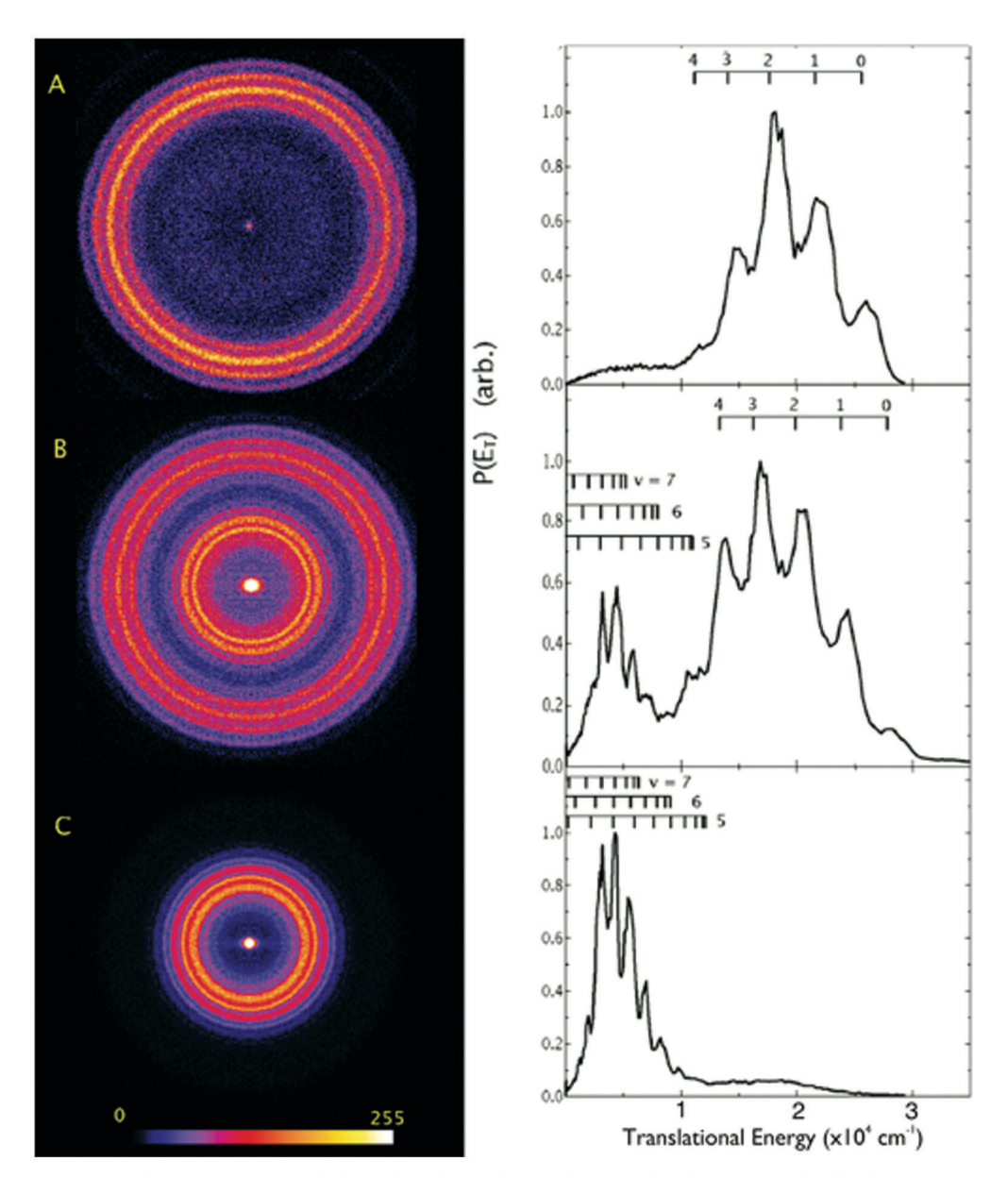


Figure 12. Velocity map images (left) and total translational energy distributions (right) for the CO (v=0) rotational levels  $j_{CO}$ =40 (A), 28 (B), and 15 (C) following photodissociation of formaldehyde in the  $S_1$   $2^14^3$  band. Combs indicate vibrational levels inferred for the undetected  $H_2$  product, except for the vibrational levels v = 5-7 associated to roaming, rotational onsets for ortho- $H_2$  are also indicated. Reproduced with permission from reference (48). Copyright 2008 American Chemical Society.

Velocity map imaging achieves measurement of photoproduct translational energies with near-spectroscopic precision, quantum state specificity and  $4\pi$  collection efficiency. This powerful combination has made state-correlated measurements in photochemistry (49) and bimolecular reactions (50) routine. Imaging studies that first revealed the roaming mechanism in formaldehyde photodissociation were built on a rich foundation of photochemical investigations spanning fifty years (51). The first excited singlet state of formaldehyde is metastable, which permits fully

rotationally resolved selective excitation. Rotationally selective fluorescence studies have reported on excited state lifetimes and suggested the presence of slow internal conversion into the electronic ground state. Two dissociative reaction pathways are thermodynamically possible: dissociation over a tight transition state (t-TS) to molecular products  $H_2$  and CO, or at slightly higher energy, barrierless simple bond fission to give radicals H + HCO. In 1993, van Zee et al. reported measurements of the CO rotational distributions following excitation of H<sub>2</sub>CO at a range of energies both below and above the onset of the radical channel (Figure 11) (52). Below the radical channel, the CO rotational distributions exhibit a Gaussian profile, and this is ascribed to the structure of the t-TS and repulsion in the exit channel. Above the radical channel this simple pattern is broken with the appearance of low rotational levels of CO. Arrows shown in Figure 11 mark j<sub>CO</sub>=40, 28 and 15 levels subjected to imaging as discussed below. These measurements strongly suggest the existence of some novel interactions as the radical threshold is crossed. Van Zee proposed two possible explanations: interaction between the radical and molecular channels, or anharmonicity of the tight transition state resulting in the formation of molecular products via some extreme geometries with much lower associated rotational excitation in CO. In retrospect, it seems that both of their explanations are correct. One might say that it is the anharmonicity of the TS associated with the opening of the radical channel that is responsible for the observations. Although this perspective affords useful insight into the transition state theory view of the measurements, the dynamics involved in this case can speak to us directly. It is the multiplexing power of imaging methods described below that permits this.

### Roaming!

Ten years after the van Zee paper, the velocity map images shown in Figure 12, obtained on selected vibration-rotation levels of CO (indicated by the arrows in Figure 11), showed that, at energies slightly above the radical channel threshold, the broken pattern in the CO rotational distributions is matched by a concomitant broken pattern in the correlated  $H_2$  vibrational distributions (47). The unexpectedly low rotational levels of CO are accompanied by a population of  $H_2$  internal states that is completely distinct from that associated with the t-TS. Extreme  $H_2$  vibrational excitation is observed, chiefly populating v=6-8. This is in contrast to the H-H distance of the t-TS, which would correspond roughly to the classical outer turning point for  $H_2$  ( $\nu$ =3). The dynamical source of this enormous vibrational excitation is obvious. It is the result of an intramolecular H + HCO reaction at long range. These observations highlight the power of state-correlated measurements made possible by the multiplexed imaging measurements. The nature of the anomalous low rotational population of CO is conclusively revealed only in the correlated  $H_2$  rovibrational distribution.

Quasiclassical trajectories then provide visualization of this extremely large amplitude motion and reveal the importance of out-of-plane trajectories for roaming (53). It was recognized immediately that having full quantum state labels on both products of such an intramolecular abstraction event was an opportunity for extraordinary insight. Careful analysis of the images shows that, although the CO rotational excitation associated with roaming is far lower than that via the t-TS, the  $H_2$  rotational distributions are considerably hotter (54). This is supported by extensive trajectory studies (55). The essential features of this story of the roaming of one H atom and the delayed abstraction event is shown in the visualization of one roaming trajectory, Figure 13, in which only the H atom motions are displayed (53). Large amplitude C-H motion precedes the roaming excursion out to 4 Å, with out-of-plane motion of the system apparent in the behavior of the formyl

H at lower left. Instantaneous force vectors are also shown beginning in times immediately preceding the abstraction. The first set of opposite-pointing arrows indicates the inner turning point of the newly formed hot  $H_2$ . Prior to the instant that configuration is reached, it is clear that these vectors are not parallel, as the formyl H is emitted with a greater tendency to follow its own O-C-H angle, while the roaming atom approaches from a less constrained direction. A related detailed investigation has recently been shown to account for bimodal CO rotational distributions associated with the formation of specific low rotational levels of  $H_2$  (56).

Although the insights into these detailed intramolecular interactions are rewarding to the dynamicist, it is the global implication of roaming in  $H_2CO$  that is most significant. These results for  $H_2CO$  suggest that any homolytic bond fission can result in products that may reorient and react at long range. Subsequent experimental and theoretical studies have confirmed this, and roaming reactions have been seen or suspected in the reaction dynamics for almost every highly excited polyatomic molecule. Any system for which the potential energy surface has an energetically accessible pair of radicals as products must be examined for the possibility of fast reaction between them that may result in closed-shell products. Very often the consequences have been unexpected.

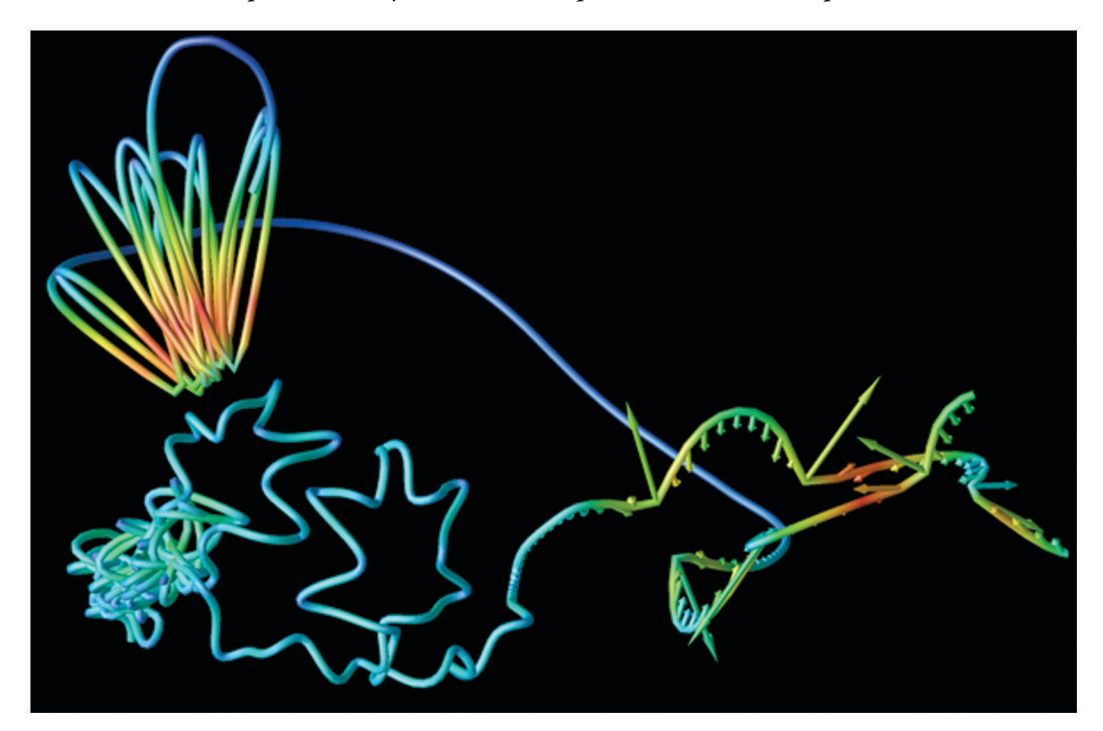


Figure 13. Visualization of a selected roaming trajectory from QCT calculations. Only H atom motions are shown, with instantaneous speed color-coded (blue is slow, red is fast). Force vectors are shown in the abstraction region at 1 fs intervals as the newly formed vibrationally excited  $\rm H_2$  departs to the right.

Reproduced with permission from reference (53). Copyright 2006 AIP Publishing.

The discovery of roaming has stimulated much theoretical work in order to reconcile roaming with transition state theory (57, 58) to treat roaming in the context of dynamical systems (59), and as theorists from other domains recast roaming in alternative terms to frame new insights (60-62). This is an active ongoing enterprise. Roaming-like behavior has been well known in ion-molecule reactions where the roaming mechanism is readily supported by the long-range ion-induced dipole

interaction and is therefore less unexpected. However, these ionic systems are also of considerable interest for theorists interested in modeling roaming dynamics (63). There has been some controversy in the literature concerning the definition of roaming behavior, and one of the present authors has suggested that the central and unexpected feature is that crucial events in reaction dynamics typically occur at long range in the van der Waals region (64).

As one might readily imagine, experimental efforts have long been made to observe roaming reactions in real time. This is challenging because, in formaldehyde, the slow internal conversion means there is a large background of the parent molecules remaining in the  $S_1$  electronic state at any given moment. This also means that it is experimentally difficult to precisely determine a time origin against which to clock the appearance of roaming products. Nevertheless, success has recently been reported using Coulomb Explosion Imaging (65). That approach, in which electrons are suddenly stripped by a strong femtosecond laser field from a system undergoing dissociation, allows reconstruction of the geometry and its time-dependence following an initial excitation by a femtosecond pulse. As CEI develops, it may combine some of the capabilities of state-correlated measurements with a time-dependent record of the dynamics. In addition to new classes of real-time probes, future directions for roaming studies include investigation of related behavior in bimolecular reactions (66) and identifying the signatures of quantum dynamics in roaming reactions (67).

### Conclusion

Molecular structure is simple. It is encoded as patterns in spectra. These patterns involve both regularly spaced spectral lines and regularly varying transition intensities. *Dynamics is seldom simple*. It is mostly encoded in broken patterns. Some broken patterns can be "fixed" by building a fit model that includes interactions between the simple bits. Some fixes can be one-offs, focusing on accidental degeneracies. Others, such as polyads, are more global, because they are based on matrix element scaling rules.

Chemical bonds are special because they are more strongly conserved than molecular geometry. But when bonds are rearranged (isomerization), broken (photolysis), or formed (reactions), it had been a deeply held belief that eigenstate-resolved spectra can give only trivial information about chemical dynamics. But this is a premature declaration/admission of defeat. We have shown in this paper that higher-order patterns (patterns of broken patterns (*hyper-patterns*), and broken patterns of broken patterns) exist that encode large amplitude motions.

Discovery and elaboration of these patterns, guided by artificial intelligence tools (e.g., XCC), can exploit both transition frequencies and intensities. Enormous quantities of raw spectral data are required. Recent experimental developments, employing techniques such as Chirped Pulse millimeter-Wave (CPmmW) spectroscopy and Velocity Mapped Imaging (VMI) are *multiplexed*. They provide multiple orders of magnitude more data (including meaningful relative intensities) per unit time. One key to multiplexed techniques is that *nothing is scanned*. Broadband techniques collect data in all frequency elements simultaneously. Resolution and signal-to-noise ratio is increased, not by scanning slowly, but instead by not scanning at all. One performs identical multiple repetitions of the same broad bandwidth data-acquisition event.

But there is another class of information that is needed in order to capture the structure and dynamics at a transition state, which involve the *correlated* motions of two (or more) semi-isolated chemical units. It is not sufficient to measure simultaneously the population distributions of two photofragments, it is necessary to measure the *correlated* distributions. What is the internal state

population distribution of photofragment A that correlates with each single state of photofragment B? CPmmW cannot but VMI can do this. These are revolutionary times!

### Acknowledgments

RWF acknowledges support from the US Department of Energy under award number DE-SC0021580 and the National Science Foundation under the grant number CHE-1800410. The research presented in this paper began when he was a graduate student in the research group of William Klemperer at Harvard more than 50 years ago, continued as a postdoc with H.P. Broida and D. O. Harris at UCSB, and grew throughout his 47-year career at MIT. Major contributions to this research were by Anthony Merer, Robert Silbey, Soji Tsuchiya, Mike Kellman, David Jonas, Kaoru Yamanouchi, Matthew Jacobson, Hai-Lung Dai, Nami Yamakita, Stefani Solina, Will Polik, Haruki Ishikawa, Steve Coy, Hans Bechtel, Jon O'Brien, Adam Steeves, Barratt Park, Joshua Baraban, Bryan Changala, and Kirill Prozument. AGS acknowledges support from the US Department of Energy under contract number DE-SC0017130, the Army Research Office under grant number W911NF-1910283, and the National Science Foundation under award number CHE-1955239. The roaming studies were built upon the seminal work in the Moore group at Berkeley, in particular the contributions by R. D. van Zee. The experimental effort was driven by Dave Townsend and Sridhar Lahankar, with theory from Joel Bowman and his group. AGS also thanks Frank Suits for the roaming visualization reproduced here as Figure 13. The formaldehyde roaming effort continues now with experimental work from Casey Foley and theory from Hua Guo and Changjian Xie.

### References

- 1. Polanyi, J. C.; Zewail, A. Direct Observation of the Transition State. *Acc. Chem. Res.* **1995**, 28, 119–132.
- 2. Lefebvre-Brion, H.; Field, R. W. *The Spectra and Dynamics of Diatomic Molecules*, Elsevier: Amsterdam, 2004, pp 62-69 and 656-671.
- 3. Huber, K. P.; Herzberg, G. *Molecular Spectra and Molecular Structure, IV. Constants of Diatomic Molecules*; Van Nostrand Reinhold: New York, 1979.
- 4. Loomis, F. W.; Wood, R. W. The Rotational Structure of the Blue-Green Bands of Na<sub>2</sub>. *Phys. Rev.* **1928**, *32*, 223.
- Launila, O.; Schimmelpfennig, B.; Fagerli, H.; Gropen, O.; Taklif, A. G.; Wahlgren, U. Spectroscopy of NbO: Characterization of the Doublet Manifold. J. Mol. Spectrosc. 1997, 186, 131–143.
- Jacobson, M. P.; Coy, S. L.; Field, R. W. Extended Cross Correlation: A Technique for Spectroscopic Pattern Recognition. J. Chem. Phys. 1997, 107, 8349–8356.
- Sparling, C.; Ruget, A.; Kotsina, N.; Leach, J.; Townsend, D. Artificial Neural Networks of Noise Removal in Data-Sparse Charged Particle Imaging Experiments. *ChemPhysChem* 2020, 21, 1–8.
- 8. Lee, K. L. K.; Patterson, J.; Burkhardt, A. M.; Vankayalapati, V.; McCarthy, M. C.; McGuire, B. A. Machine Learning of Interstellar Chemical Inventories. *The Astrophysical Journal Letters* **2021**, *917*, L6.
- 9. Herzberg, G. Molecular Spectra and Molecular Structure. I. Spectra of Diatomic Molecules; Van Nostrand: Princeton, 1950; pp 175-185

- 10. Field, R. W.; Baraban, J.; Lipoff, S. H.; Beck, A. R. Effective Hamiltonians in *Handbook of High-Resolution Spectroscopies*; Quack, M., Merkt, F., Eds.; John Wiley & Sons, 2010.
- 11. Renhorn, I. Cambridge, MA, 1976, private communication.
- 12. Kovács, I. Rotational Structure in the Spectra of Diatomic Molecules; Elsevier: New York, 1969.
- 13. Field, R. W.; Wicke, B. G.; Simmons, J. D.; Tilford, S. G. Analysis of Perturbations in the a<sup>3</sup> ∏ and A<sup>1</sup> ∏ States of CO. *J. Mol. Spectrosc.* **1972**, *44*, 383–399.
- 14. Field, R. W. Assignment of the Lowest  ${}^{1}\Pi$  and  ${}^{3}\Pi$  States of CaO, SrO, and BaO. *J. Chem. Phys.* **1974**, *60*, 2400–2413.
- 15. Field, R. W.; Lagerqvist, A.; Renhorn, I. The Low Lying Electronic States of SiO. *Physica Scripta* **1976**, *14*, 298–319.
- 16. Lefebvre-Brion, H.; Field, R. W. *The Spectra and Dynamics of Diatomic Molecules*; Elsevier: Amsterdam, 2004; Section 6.5.2, pp 418-427.
- 17. Gelbart, W. M.; Freed, K. F. Intramolecular Perturbations and the Quenching of Luminescence in Small Molecules. *Chem. Phys. Lett.* **1973**, *18*, 470–475.
- 18. Darling, B. T.; Dennison, D. M. The Water Vapor Molecule. Phys. Rev. 1940, 57, 128–139.
- 19. Kellman, M. E. Approximate Constants of motion for vibrational spectra of many-oscillator systems with multiple anharmonic resonances. *J. Chem. Phys.* **1990**, *93*, 6630–6635.
- 20. Fried, L. E.; Ezra, G. S. Semiclassical quantization using classical perturbation theory: Algebraic quantization of multidimensional systems. *J. Chem. Phys.* **1987**, *86*, 6270–6282.
- 21. Kellman, M. E.; Chen, G. Approximate constants of motion and energy transfer pathways in highly excited acetylene. *J. Chem. Phys.* **1991**, *95*, 8671–8672.
- 22. Kellman, M. E.; Xiao, L. New Assignment of vibrational spectra of molecules with the normal to local modes transition. *Chem. Phys. Lett.* **1989**, *162*, 486–490.
- 23. Jacobson, M. P.; O'Brien, J. P.; Silbey, R. J.; Field, R. W. Pure Bending Dynamics in the Acetylene  $\widetilde{X}^1\Sigma^+$  State to 15,000 cm<sup>-1</sup> of Internal Energy. *J. Chem. Phys.* **1998**, *109*, 121–133.
- 24. Jacobson, M. P.; Field, R. W. Acetylene at the threshold of isomerization. *J. Phys. Chem. A* **2000**, *104*, 3373–3386.
- Merer, A. J.; Steeves, A. H.; Baraban, J. H.; Bechtel, H. A.; Field, R. W. Cis-trans isomerization in the S<sub>1</sub> state of acetylene: identification of cis-well vibrational levels. J. Chem. Phys. 2011, 134, 244310.
- Baraban, J. H.; Changala, P. B.; Mellau, G. C.; Stanton, J. F.; Merer, A. J.; Field, R. W. Spectroscopic Characterization of Isomerization Transition States. Science 2015, 350, 1338–1342.
- Kittrell, C.; Abramson, E.; Kinsey, J. L.; McDonald, S.; Reisner, D. E.; Katayama, D.; Field, R. W. Selective Vibrational Excitation by Stimulated Emission Pumping. J. Chem. Phys. 1981, 75, 2056–2059.
- Jonas, D. M.; Solina, S. A. B.; Rajaram, B.; Silbey, R. J.; Field, R. W.; Yamanouchi, K.; Tsuchiya, S. Intramolecular Vibrational Relaxation and Forbidden Transitions in the SEP Spectrum of Acetylene. *J. Chem. Phys.* 1992, 97, 2813–2816.
- Jonas, D. M.; Solina, S. A. B.; Rajaram, B.; Cohen, S. J.; Silbey, R. J.; Field, R. W.; Yamanouchi, K.; Tsuchiya, S. Intramolecular Vibrational Relaxation in the SEP Spectrum of Acetylene. J. Chem. Phys. 1993, 99, 7350–7370.

- 30. Williams, S.; Tobiason, J. D.; Dunlop, J. R.; Rohlfing, E. A. Stimulated Emission Pumping Spectroscopy via Two-Color Resonant Four-Wave Mixing. *J. Chem. Phys.* **1995**, *102*, 8342–8358.
- 31. Solina, S. A. B.; O'Brien, J. P.; Field, R. W.; Polik, W. F. Dispersed Fluorescence Spectrum of Acetylene from the  $\tilde{A}^1A_u$  Origin: Recognition of Polyads and Test of Multiresonant Effective Hamiltonian Model for the X State. *J. Phys. Chem.* **1996**, *100*, 7797–7809.
- 32. O'Brien, J. P.; Jacobson, M. P.; Sokol, J. J.; Coy, S. L.; Field, R. W. Numerical Pattern Recognition Analysis of Acetylene Dispersed Fluorescence Spectra. *J. Chem. Phys.* **1998**, *108*, 7100–7113.
- Steeves, A. H.; Bechtel, H. A.; Merer, A. J.; Yamakita, N.; Tsuchiya, S.; Field, R. W. Stretch-bend Combination Polyads in the ùAu State of Acetylene, C2H2. J. Mol. Spectrosc. 2009, 256, 256–278.
- 34. Baraban, J. H.; Stanton, J. F.; Merer, A. J.; Field, R. W. Anharmonic Force Fields of *cis* and *trans*-S<sub>1</sub> C<sub>2</sub>H<sub>2</sub>. *Mol. Phys.* **2012**, *110*, 2725–2733.
- 35. Wiberg, K. B.; Rablen, P. R.; Baraban, J. H. Butadiene and Heterodienes Revisited. *J. Org. Chem.* **2018**, 83, 8473–8482.
- 36. Baraban, J. H.; Martin-Drumel, M.-A.; Changala, P. B.; Eibenberger, S.; Nava, M.; Patterson, D.; Stanton, J. F.; Ellison, G. B.; McCarthy, M. C. The molecular structure of gauche-1,3-butadiene: Experimental establishment of non-planarity. *Angewandte Chemie Internatl. Ed.* **2018**, *57*, 1821–1825.
- 37. Anslyn, E. V.; Dougherty, D. A. *Modern Physical Organic Chemistry*; University Science Books, 2006; pp 401-402. The authors state that "Throughout the 20th century it was a cornerstone of mechanistic analysis that we could never "see" a transition state ... we remain in the classical situation in which it is experimentally impossible to characterize a transition state."
- 38. Stanton, J. F.; Huang, C.-M.; Szalay, P. G. Stationary Points on the S<sub>1</sub> Potential Energy Surface of C<sub>2</sub>H<sub>2</sub>. *J. Chem. Phys.* **1994**, *101*, 356–365.
- Prozument, K.; Baraban, J. H.; Changala, P. B.; Park, G. B.; Shaver, R. G.; Muenter, J. S.; Klippenstein, S. J.; Chernyak, Y. V.; Field, R. W. Photodissociation Transition States Characterized by Chirped-Pulse Millimeter-Wave Spectroscopy. *Proc. Natl. Acad. Sci.* 2020, 117, 146–151.
- Prozument, K.; Shaver, R. G.; Ciuba, M. A.; Muenter, J. S.; Park, G. B.; Stanton, J. F.; Guo, H.; Wong, B. M.; Perry, D. S.; Field, R. W. A New Approach Toward Transition State Spectroscopy. *Farad. Disc.* 2013, 163, 33–57.
- 41. Brown, G. G.; Dian, B. C.; Douglass, K. O.; Geyer, S. M.; Shipman, S. T.; Pate, B. H. A broadband Fourier transform microwave spectrometer based on chirped pulse excitation. *Rev. Sci. Instrum.* **2008**, *79*, 053103.
- Chang, C.-H.; Nesbitt, D. J. Spectroscopy and dynamics of jet-cooled polyynes in a slit supersonic discharge: Sub-Doppler infrared studies of diacetylene HCCCCH. J. Phys. Chem. A 2015, 119 (28), 7940–7950.
- 43. Loh, Z.-H.; Field, R. W. Contrasting origins of the isomerization barriers for vinylidene, fluorovinylidene, and difluorovinylidene. *J. Chem. Phys.* **2003**, *118* (9), 4037–4044.

- 44. Chandler, D. W.; Houston, P. L. Two-dimensional imaging of state-selected photodissociation products detected by multiphoton ionization. *J. Chem. Phys.* **1987**, 87 (2), 1445–1447.
- 45. Eppink, A. T. J. B.; Parker, D. H. Velocity map imaging of ions and electrons using electrostatic lenses: Application in photoelectron and photofragment ion imaging of molecular oxygen. *Rev. Sci. Instrum.* **1997**, *68* (9), 3477–3484.
- 46. Suits, A. G. Invited review article: photofragment imaging. *Rev. Sci. Instrum.* **2018**, 89 (11), 111101.
- Townsend, D.; Lahankar, S. A.; Lee, S. K.; Chambreau, S. D.; Suits, A. G.; Zhang, X.; Rheinecker, J.; Harding, L. B.; Bowman, J. M. The Roaming Atom: Straying from the Reaction Path in Formaldehyde Decomposition. Science 2004, 306 (5699), 1158–1161.
- 48. Suits, A. G. Roaming Atoms and Radicals: A New Mechanism in Molecular Dissociation. *Acc. Chem. Res.* **2008**, *41* (7), 873–881.
- 49. Komissarov, A. V.; Minitti, M. P.; Suits, A. G.; Hall, G. E. Correlated product distributions from ketene dissociation measured by dc sliced ion imaging. *J. Chem. Phys.* **2006**, *124*, 014303.
- 50. Lin, J. J.; Zhou, J. G.; Shiu, W. C.; Liu, K. P. State-specific correlation of coincident product pairs in the F+CD<sub>4</sub> reaction. *Science* **2003**, *300* (5621), 966–969.
- 51. Moore, C. B.; Weisshaar, J. C. Formaldehyde photochemistry. *Ann. Rev. Chem. Phys.* **1983**, 34, 525–55.
- 52. van Zee, R. D.; Foltz, M. F.; Moore, C. B. Evidence for a Second Molecular Channel in the Fragmentation of Formaldehyde. *J. Chem. Phys.* **1993**, *99* (3), 1664–1673.
- 53. Lahankar, S. A.; Chambreau, S. D.; Townsend, D.; Suits, F.; Farnum, J.; Zhang, X.; Bowman, J. M.; Suits, A. G. The roaming atom pathway in formaldehyde decomposition. *J. Chem. Phys.* **2006**, *125* (4), 044303/1–044303/10.
- 54. Suits, A. G.; Chambreau, S. D.; Lahankar, S. A. State-correlated DC slice imaging of formaldehyde photodissociation: roaming atoms and multichannel branching. *Int. Rev. Phys. Chem.* **2007**, 26 (4), 585–607.
- Houston, P. L.; Conte, R.; Bowman, J. M. Roaming Under the Microscope: Trajectory Study of Formaldehyde Dissociation. *J. Phys. Chem. A* 2016, 120, 5103–5114.
- Quinn, M. S.; Nauta, K.; Jordan, M. J.; Bowman, J. M.; Houston, P. L.; Kable, S. H. Rotational resonances in the H<sub>2</sub>CO roaming reaction are revealed by detailed correlations. *Science* 2020, 369 (6511), 1592–1596.
- Klippenstein, S. J.; Georgievskii, Y.; Harding, L. B. Statistical Theory for the Kinetics and Dynamics of Roaming Reactions. J. Phys. Chem. A 2011, 115 (50), 14370–14381.
- 58. Andrews, D. U.; Kable, S. H.; Jordan, M. J. T. A Phase Space Theory for Roaming Reactions. *J. Phys. Chem. A* **2013**, *117* (32), 7631–7642.
- 59. Mauguière, F. A.; Collins, P.; Kramer, Z. C.; Carpenter, B. K.; Ezra, G. S.; Farantos, S. C.; Wiggins, S. Roaming: A phase space perspective. *Ann. Rev. Chem. Phys.* **2017**, *68*, 499–524.
- Mauguiere, F. A. L.; Collins, P.; Kramer, Z. C.; Carpenter, B. K.; Ezra, G. S.; Farantos, S. C.; Wiggins, S. Phase Space Structures Explain Hydrogen Atom Roaming in Formaldehyde Decomposition. *J. Phys. Chem. Lett.* 2015, 6 (20), 4123–4128.
- 61. Bowman, J. M.; Houston, P. L. Theories and simulations of roaming. *Chem. Soc. Rev.* **2017**, 46 (24), 7615–7624.

- 62. Cofer-Shabica, D. V.; Stratt, R. M. What is special about how roaming chemical reactions traverse their potential surfaces? Differences in geodesic paths between roaming and non-roaming events. *J. Chem. Phys.* **2017**, *146* (21), 214303.
- 63. Mauguière, F. A.; Collins, P.; Ezra, G. S.; Farantos, S. C.; Wiggins, S. Multiple transition states and roaming in ion–molecule reactions: a phase space perspective. *Chem. Phys. Lett.* **2014**, *592*, 282–287.
- 64. Suits, A. G. Roaming Reactions and Dynamics in the van der Waals Region. *Ann. Rev. Chem. Phys.* **2020**, *71*, 77–100.
- Endo, T.; Neville, S. P.; Wanie, V.; Beaulieu, S.; Qu, C.; Deschamps, J.; Lassonde, P.; Schmidt, B. E.; Fujise, H.; Fushitani, M. Capturing roaming molecular fragments in real time. Science 2020, 370 (6520), 1072–1077.
- 66. Li, H.; Suits, A. G. Universal crossed beam imaging studies of polyatomic reaction dynamics. *Phys. Chem. Chem. Phys.* **2020**, 22 (20), 11126–11138.
- 67. Li, A.; Li, J.; Guo, H. Quantum Manifestation of Roaming in H + MgH → Mg + H<sub>2</sub>: The Birth of Roaming Resonances. *J. Phys. Chem. A* **2013**, *117* (24), 5052–5060.